FINAL TECHNICAL REPORT

on

EFFECT OF ENVIRONMENT IN FATIGUE OF COPPER CRYSTALS

BY

Dr. Irwin Greenfield

Submitted to

National Aeronautics and Space Administration
Office of Scientific & Technical Information
Washington, D.C. 20546

SU-DMS-71-T-15

Part I Apparatus

INTRODUCTION

The nucleation of fatigue cracks apparently occurs on the surface or near the surface of the material tested. The series of experiments that will be described in these reports will be concerned with the evaluation of the effects of surfaces and environment on the nucleation and growth of fatigue cracks. The material chosen was copper because of the large amount of quantitative information about this face-centered-cubic metal found in the literature. In order to change the surface characteristics, gold was diffused a short distance into the surface; environmental changes were accomplished by conducting the fatigue tests in vacuum (10^{-7} torr) or in oxygen (50 torr).

The fatigue machine was specifically developed for these tests and was a constant total strain amplitude device. Since a reverse bend fatigue test on single crystals of about 1.0 mm thick was employed, the cycling device produced oscillating loads of less than 500 grams. A measuring system was developed to record the load applied and the strain amplitude during the fatiguing of the specimen.

Design and Construction of Apparatus

Figure 1 is a block diagram of the fatigue apparatus. The single crystal cantilever specimen is contained in a chamber that can be evacuated or filled with the desired atmosphere. The load is applied through a proving ring by a vertical rod extending to the transmission which converts rotary motion into reciprocating motion. The amplitude displacement from this gear box is adjustable to a maximum of 3mm. The cyclic frequency is adjusted by using a servo motor in conjunction with a Master Motor Control manufactured by Electrocraft. The frequencies used in these tests were between 20 and 60 cps. Several proving rings were employed in these experiments; they were designed to measure loads up to 500 grams with a minimum of vertical deflection. By placing an iron core along the displacement rod and using a Hewlett-Packard DCDT, the translation of the rod was continuously monitored. This displacement signal was directly noted on an oscillo-

scope so that fine adjustments of the amplitude of the displacement were possible. The cyclic wave produced was sinusodal.

Figure 2 shows the environment chamber opened; the specimen, clamp and proving ring are shown. The diameter of the proving ring is about 1.5 inches. The bottom of the closed chamber is shown in Figure 3. The arrangement of the servo motor, transmission and DCDT are shown clearly. In order to adjust the vertical rod so that the cantilever deflected symmetrically about its neutral axis, a differential screw was introduced above the DCDT. This is indicated by mechanical zero in Figure 3.

The load was monitored in several ways. The signal from the proving ring was amplified by a Burr-Brown strain gage amplifier and observed on the cscilloscope. If the displacement signal is connected to the X terminal and the load signal is connected to the Y terminal of the oscilloscope, a hysteresis trace will result. Thus, the oscilloscope can be used to follow the dynamic changes during the test. In order to obtain a permanent record of the change in load, the amplified signal from the proving ring was rectified by a bridge rectifier and then recorded on a millivolt strip-chart recorder. The recorder was on during the entire life of the specimen and was adjusted to turn off the motor when the specimen broke or a given drop of load occurred.

In order to electrically adjust the neutral position of the cantilever beam a D.C. millivolt meter was introduced into the circuit. For symmetrical bending, the voltage produced at the maximum and minimum deflection amplitudes is equal and opposite. A frequency counter and total cycle counter was used so that the frequency was adjusted accurately and the total number of cycles was recorded. Although the system was adequate for these preliminary experiments, some improvements on the mechanical and electronic system are desirable for the future work.

Specimen:

Single crystals of high purity copper (99.999%), grown by a Bridgeman technique, were used as specimens. In order to develop a constant shear stress

on the slip system on the surface of the crystal, the crystals were grown as a tapered beam of a thickness of 1.0 mm and a length of about 5.0 cm. The width was tapered 10° so that in the gage length the width increased from 2.8 mm to 10.9 mm.

Assuming a simple beam theory the stresses σ_{11} and σ_{12} are found to be

$$\sigma_{11} = - \frac{12 P_2 x_1 x_2}{W(x_1) h^3}$$

$$\sigma_{12} = - \frac{6 P_2}{W(x_1) h^3} \left(\frac{h^2}{4} - x_2^2 \right)$$

where the free end of the cantilever beam is the origin of the coordinate system and x_2 (distance in the thickness direction) is measured from the neutral axis. The force P_2 is applied to the free end of the beam. The thickness of the crystal is h while $W(x_1)$ is the width as a linear function of a distance along the length.

If the resolved shear stress on the slip plane is given by

then $$\sigma_{ij} = \alpha_{ik} \alpha_{j\ell} \sigma_{k\ell} = \sigma_{12}'$$

$$\sigma_{12}^{1} = \alpha_{11} \alpha_{12} \sigma_{11} + (\alpha_{11} \alpha_{22} + \alpha_{11} \alpha_{21}) \sigma_{21}$$

or

$$\sigma_{12}^{1} = - \frac{6 P_2}{h^3} \left[\frac{2 x_1 x_2 \alpha_{11} \alpha_{21}}{W(x_1)} + \left(\frac{h^2}{4} - x_2^2 \right) (\alpha_{11} \alpha_{22} + \alpha_{12} \alpha_{21}) \right]$$

At or near to the surface $x_2 \simeq \frac{h}{2}$ and the second term in the brackets is small and assumed to be zero. Thus, the resolved shear stress in the surface layers is then

$$\alpha_{12}' = - \frac{6P_2}{h^2} \frac{x_1}{W(x_1)} \alpha_{11} \alpha_{21}$$

Since $\frac{6x_1}{W(x_1)}$ is constant for all specimens then

$$\sigma_{12}' = - \frac{P_2 C \alpha_{11} \alpha_{21}}{h^2}$$

is the resolved shear stress for various thickness. A more complete description of the stress distribution for this shape of specimen leads to nearly the same results.*

All crystals were annealed in a high vacuum for 48 hours at 780°C, then electropolished in preparation for the fatigue or the coating of gold. A layer of 500Å of gold was vapor deposited onto two opposite faces of one group of specimens. These were diffusion-annealed to create thin solute layers. Using diffusion data extrapolated to the annealing temperature employed in this experiment, a profile of composition near the surface was determined; the surface composition is about 0.11 while $2\sqrt{Dt}$ is about 0.54 μ. See figure 5.

After these treatments the specimens were stored in a dry atmosphere until tested.

* Figure 4 is a plot of the maximum stress at the specimens surface. It is noted that at the narrow end the stress level is low. The stress is nearly constant, however, throughout the major portion of the beam.

EFFECT OF ENVIRONMENT IN FATIGUE OF COPPER CRYSTALS

INTRODUCTION TO PART II

Single crystals of high purity copper were fatigued at low strain amplitudes of about 10^{-4} in various environments. The tests were conducted in vacuum (10^{-7} torr) or in oxygen (50 torr). The surface conditions of the copper crystals were altered for some of the tests by creating a diffusion layer of gold that extended about 2000 Å below the surface.

The fatigue apparatus was designed to give constant displacement in flexure. During the tests, the hardening and energy loss as a function of the number of cycles were recorded. In addition, optical and scanning electron microscope observations of the surfaces were made at the end of the tests. Part I of this report is a discussion of the apparatus, experimental design and the sensitivity of the system. Part II is concerned with microscope observations of the surfaces after treatments; and Part III is a presentation of the experimental-mechanical data.

PART II: OBSERVATIONS OF SURFACES OF FATIGUED COPPER CRYSTALS.

1. Optical Microscopy

1.1 Pure copper single crystals fatigued in oxygen

The optical microscope investigation of the surface of the fatigued specimen after the tests showed relatively clear surfaces, free of slip markings or persistant slip lines except near the region of the fracture. Within 0.5mm of the fracture many slip-line-like striations, most of which corresponded to the primary slip system were observed. In the optical microscope, however, the character of the lines were quite different from the appearance of ordinary slip lines since the observed linear patterns contained serrated irregular markings. Figure 6 is a composite showing the arrangement of the serrated-slip lines near the fracture surface. (The orientation of this crystal, specimen 12, is shown in Figure 7.) The density of the serrated slip lines increases from several clusters until the entire surface is covered near the fracture surface.

The regions between the serrated slip clusters are shown clearly in Figure 8; fine lines parallel to the primary lines are seen. In addition, a secondary pattern is also noted in 8a. Small serrations are arranged in a linear array in a direction which, for the most part, is parallel to the cross slip direction. In Figure 8b, an area taken from another part of this specimen, these serrations are aligned generally along a direction which is defined by the critical slip system (see A in Figure 8b). These serrations were identified clearly as extrusions by scanning electron microscopy.

In the region adjacent to a small grain which was found in the crystal, the pattern of lines shows that three slip systems, primary, cross, and critical, were active during fatigue. This is illustrated in Figures 9 and 10. Since the intersection of the primary and conjugate systems with the surface result in nearly parallel lines, these two systems can not be identified independently.

2. Scanning Electron Microscopy

2.1 Pure crystal fatigued in oxygen

Many of the gross features observed on copper fatigued in oxygen are similar to those when the tests were carried out in high vacuum. In a later section of this report, the differences will be discussed.

The scanning electron microscope photomicrographs gave excellent detail of the serrated slip lines. Figure 11a is a low magnification of the surface, near the fracture, which contained many surface lines. It is obvious that the characteristics of these lines are different than the slip lines which are produced by non-cyclic plastic deformation. Extrusions are in profusion. In fact all surface lines in this photomicrograph contain extrusions. These structures are developed on the primary slip lines; however, a second pseudo-orientation relating the positions of the extrusions is observed. These patterns can be seen at A of Figure 11 a. Figure 11b is a higher magnification. Two types of extrusions are present; in the area of a cluster of primary lines at A, the extrusions have a braided appearance (see Figures 11b and 11d). In narrow striations however, the extrusions do not have the braided appearance and they are clearly elongated in the direction of the Burgers vector. This condition is shown in Figure 11c; the Burgers vector is denoted by B. The extrusions are always aligned along slip planes within or adjacent to valleys in the surface. These valleys correspond to intrusions. In addition to the activity on the primary slip system, faint cross slip lines can be see at A in Figure 11c. In certain regions there seems to be a relationship between the spacing of the intrustions and the intersections of the cross slip system.

Careful observations of these extrusions reveal that the extrusion tongues are a laminate of several layers of metal in a composite-like structure. This arrangement is shown clearly in Figures 12a and 12b at L. The extrusion at A seems to have been squeezed from the valley and has been bent over in the process. The intrusions, I, are quite long and appear to be deep. The edge at the intersections of intrusions with the surface have rounded corners unlike slip lines. A small intrustion, I, is observed in Figure 12c with no corresponding extrusion. This kind of observation is less frequent than the long valley-like intrusions

that contain many extrusions.

Figure 13 (as the optical micrograph in Figure 10) illustrates the structure resulting from two active slip systems. The large extrusions and deep valleys are a result of deformation on the primary system, P; the cross slip is more closely spaced and is indicated by C. At A, one can see the effect of the combined slip on the primary and cross slip system which produced a displacement of a segment of material in the direction of the common Burgers vector. In Figure 13b another characteristic of the extrusions is clearly shown. While slip and fatigue striations occurred on the cross slip system, the cross slip lines gradually disappear on the extrusion. Since the surface of the extrusion is essentially the primary slip plane and the Burgers Vector is the same in both primary and cross slip systems, slip steps in the surface will not be produced. The ridge of the extrusion should, however, show displacements if cross slip action took place. Later it will be shown that for copper fatigued in high vacuum, a finer structure is observed on these extrusions.

Interfaces, such as grain boundaries have been found to affect the development of extrusions. Figures 14a and 14b show SEM photomicrographs at two magnifications of a grain boundary, G. Near the boundary, in the crystal that was oriented for maximum shear stress on one plane, extrusions occur in the primary slip system, Ep. Other stresses are present which cause some plastic activity on the secondary slip systems. At the boundary, however, large extrusions not associated with any of the slip planes appear. This observation indicates that extrusion producing activity is present at grain boundaries in addition to the slip planes. It will be shown later that similar observations are made near surfaces coated with a diffused layer of solute.

The intersection between the fracture surface and the specimen surface reveals some aspects concerning the progress of the fatigue crack and details of a portion of extrusions which extended into the intrusion valleys. In Figure 15, the fracture is step-like near the specimen surface and follows the primary and cross slip planes. At higher magnification (Figure 15b) the arrangement of the extrusions on the specimen surface at the fracture can be seen. Extrusion activity is conspicuous in the primary bands near the fracture

surface (see E in Figure 15c). The crack apparently travelled along the valley that was adjacent to the extruded regions. On the cross-slip-fracture faces, however, no obvious evidence of extrusions are noted. Other cracks, usually extending along the primary slip system, are also visible in Figure 11b.

If, in the scanning electron microscope, the specimen is oriented with the fracture surface about 30° from the plane of view, the intersection between the specimen surface and the fracture surface can be better studied. Because of the angle of observation, the topography of the specimen surface is accentuated. The image resulting from this arrangement is shown in Figure 16. The arrow F lies along the intersection of these two surfaces; the top of the photomicrograph is the original specimen surface. Along F are extrusions which extend more than 5μ into the fracture. In this region the depth of stage I crack growth seems to coincide with the depth of the extrusions. On the specimen surface, not only is there evidence of severe primary slip activity, but extended cross slip lines, some containing extrusions as long as 20μ are prominent. The effect of cross slip is seen clearly along the heavy ridge which traverses the middle of the photograph. In front of this ridge, some of the primary extrusions appear to be aligned along the cross slip direction. The apparent depression in the upper part of the photograph is probably a polishing pit.

Another area showing the boundary between the fracture surface and the specimen surface is shown in Figure 17. The fracture surface, within 10μ of the specimen surface, is along the primary slip planes. Some of the extrusions extend as far as 5μ into the fracture surface; these extrusions are clearly seen at the higher magnification in Figure 17b. In Figure 17a, a crack can be seen on the border between a region where one slip system is active and a region where two systems are active. This crack can be traced into the fracture surface. The secondary system that is seen in these photographs is the critical slip system indicated by M. Since the activity on this system was intense in this region and the view of the specimen is almost directly along the critical plane, any cross slip which may have occurred is concealed. However, the critical system activity which apparently took place after some of the primary extrusions developed, displaced the primary extrusions to form the spire-like structure.

Figure 18 is another region of the fracture surface. The fracture progressed along the primary and a secondary slip plane. At higher magnification remnants of extrusions are seen in the fracture surface.

A photograph of a large extrusion extending about 8μ out of the specimen surface is shown in Figure 19. The general topography in the background is due to many smaller extrusions.

2.2 Fatigue in Vacuum

The scanning electron micrographs of the surface after fatigue in a vacuum of 10^{-7} torr show some differences in structure than those observed on specimens fatigued in oxygen. Figure 20 is a low magnification SEM photograph of the surface. The extrusions appear to be as prevalent as in the specimens fatigued in oxygen, but the somewhat orderly spacing of the extrusions is not observed. Compare with Figure 11a. In the region between the cluster of slip striations, there is faint evidence of slip lines S which do not contain extrusions. In Figure 20b clear slip lines, S appear near to heavily extruded regions, E. Extrusions have developed, however, in the slip lines at E in Figure 20b. A second slip system was also active during the fatigue and this is seen at C in the photograph.

Figure 21 shows the surface of the fatigued specimen more clearly. The lack of uniformity is also seen here. A secondary system is active, but its effect is different from that in the specimen fatigue in oxygen. In the vicinity of A in the photomicrographs, b and c, a fine serrated structure on the ridge of the extrusion can be seen. The extrusions are quite structured with fine spires along the edges. As pointed out before, the structure on the ridge of the extrusion can be due to secondary slip action. Another difference is noted. The laminates of the extrusions are clearly defined (see Figure 21c area B). Thus, in general, a fine structure which is not seen in the specimens fatigued in oxygen is present in specimens fatigued in high vacuum.

In certain portions of the specimen, cross slip appeared to be very

active. Figure 22a and 22b are examples of these regions. The primary slip shown in 22b has been displaced by the action of the cross slip region. Although not too clear, some extrusions can be seen on the cross slip system.

2.3 Effects of diffused coatings on the surface of copper single crystals.

The thin diffused layer was produced by annealing crystals with a 200Å evaporated coating of gold so that a solute affected region of about 1000Å was developed. This diffused layer had a considerable effect on the characteristics of the surface structure produced by fatigue. Slip lines or fatigue striations were rare on the surface and only few were found in the vicinity of the fracture. Figures 23a and 23b show these striations. The extrusions observed however, are rather long and often oddly shaped. Extrusion free regions found along the slip striations may be due to the breaking of the extruded material during the fatigue. The fracture surface near the surface of the specimen corresponds to the (111) planes although it is not as distinct as in the uncoated specimens. A fracture is shown in Figure 24.

The study of the intersection between the fracture surface and the specimen surface proved to be quite instructive. Figure 25 is a view of the fracture surface. Although a diffused zone is produced by the annealing treatment, this photomicrograph reveals at the specimen surface a crust-like formation about 0.2 to 0.3μ thick. At the interface between the crust and the bulk material are found a profusion of extrusions, E. Moreover, some extrusions are found near the interface on the fracture surface at E'. The extrustion from the interface is clearly shown in Figures 26a and 26b. In Figure 26a the extrusion is over 20μ in length in one portion. This unique feature which is present at the interface is similar to the extruded material seen at the grain boundaries. Thus, in a surface hardened crystal, although there is very little plastic deformation activity throughout the layer itself, the activity under the layer must be large. It appears that crust deforms, in general, elastically, whereas, the material directly below the surface deforms plastically.

3. Discussion

It has been shwon that extrusions and intrusions form in profusion on the surface of a fatigues, uncoated, copper single crystal. The characteristics of this structure after low strain amplitude fatigue can be summarized by the following:

A. General observations for uncoated copper specimens

   a. Extrusions and intrusions are abundant along the primary slip system in the high stress regions.
   b. Secondary slip systems, especially cross slip are active.
   c. Some extrusions occur on the cross slip system. (intrusion probably occur also)
   d. Displacements along the secondary system tends to modulate the shape of the primary extrusions.
   e. In certain areas of the specimen surface there is a secondary orientation relationship between the extrusions; cross slip seems to be a factor.
   f. The extrusions consist of layers of material, each layer about 0.1μ thick.
   g. The extrusions are elongated in the direction of the Burgers vector.

B. Contrast between specimens fatigued in oxygen and those fatigued in vacuum.

   a. The laminate-like structure of the extrusions are not as clearly defined when developed in oxygen as when developed in vacuum.
   b. Sharp spires appear in vacuum fatigue but are not seen in the oxygen fatigue.

C. Thin-surface alloy layer observations

   The surfaces after fatigue are different from those observed on the pure copper crystals.

   a. A definite surface crust less than 5000 Å thick is observed.

b. This crust is not plastically deformed except for several isolated slip lines which intersected the fracture surface.

c. Under the crust, however, considerable plastic deformation takes place which is indicated by large extrusions, that appear on the fracture surface after fracture.

In order to discuss the development of the surface structure during fatigue observed mechanical properties and the dislocation structure near the surface must be considered. Details on the mechanical properties will be presented in Part III of this report, whereas; the dislocation arrangements will be discussed on the basis of previous published results.

Extrusion and intrusion along the primary and secondary slip lines, first observed and explained by Cottrell and Hull[1], are the most prominent feature observed on the surface of the specimens not diffusion coated. The extrusions are elongated in the direction of the Burgers vector. Intrusions, on the other hand, seem more continuous and have the appearance of long valleys extending some distance along the slip planes. Replica evidence however, has shown that the shapes of the boundaries of the intrusions are similar to the shapes of the extrusions[1]. The depths of the intrusions are often greater than 10μ; these structures are associated with the persistant striations[2,3,4]. The edge of the fracture face near the surface of the specimen is usually along the primary and secondary slip planes. Obviously, the surface notches produced by long intrusions are primary for the initiation of the fatigue cracks.

Because of the details that are observed by the SEM, the mechanisms of extrusion and intrusion development can be further clarified. Thin film electron microscopy showed that during cyclic straining, a dislocation cell structure forms[4,5]. If the primary slip system is $(11\bar{1})$ $[101]$ then, in the early stages of fatigue, the cell structure consists of veins along the $[121]$[16]; this structure then develops into a large dislocation cell configurtion. During this period of build-up of the dislocation density, the flow stress of the material steadily increases while the hysteresis curves indicate large energy losses. (The significance of the energy loss data will be discussed in Part III of the report.) Apparently when the area of the hysteresis

curves decreases to a minimum, the dislocation cell structure also reaches a steady state of a somewhat constant mesh size. Althought the internal distribution of dislocations is not greatly affected after the establishment of steady-state, large numbers of extrusions and intrusions form-in-the highly stressed regions of the specimen. Dislocation movement in each cycle, however, must be relatively small since the energy loses are small.

Consider the number of dislocation that would be involved in the formation of an extrusion of average size, say 0.1μ wide, 3μ high and 10μ long. If the dislocation source, ten microns long and two opposite edge dislocations 1000 Å apart in the form of a dipole, is considered, then the volume transferred which occurs when the dislocation dipole reaches the surface is about

$$3 \times 10^{-16} \text{ cm}^3 / \text{ dipole}$$

For an average size extrusion the volume is

$$3 \times 10^{-12} \text{cm}^3 / \text{ extrusion}$$

The number of dislocation dipoles to reach the surface is then

$$\frac{3 \times 10^{-12} \text{cm}^3/\text{extrusion}}{3 \times 10^{-16} \text{cm}^3/\text{dipole}} = 1000 \text{ dipoles/extrusion}$$

The association of dipoles with intrustion and extrusions has been suggested by Chen, Gilman and Head[7]. They calculated the binding energy of several arrangements of dipoles, tripoles and quadrupoles and concluded that in fatigue conditions these configurations can decompose. The binding energy for the array depends upon the geometry of the configuration.

The cell structure of dislocations that is produced during fatigue is likely to be a combination of opposite types of dislocations aligned in veins[6]; thus this structure should be of the form of a large multiple with a net Burgers vector of either zero or very small. A possible ideal dislocation arrangement is shown in Figure 27. The dislocations around the perifery of the vein are easier to remove than those in the interior. Thus, an applied shear stress will displace the outer dislocations before affecting

those inside the vein. Consider columns AC and BD in Figure 27. This is reproduced in different perspective in Figure 28. If A', B', C' and D' are pinning points in the cell wall, and the length AA' and BB' are one half the dislocation source length, then the effect of stress on these dislocations can be discussed. Since the outer-most dislocation is the least bound, during the first half of the stress cycle τ_2, the next nearest dislocations are displaced in the same directions as the other half of the dipole. At the surface opposite AA' and BB' an intrusion, one Burgers vector in depth, will form; whereas, opposite CC' and DD' an extrusion will occur. The dipole that was removed from the bottom of the vein is likely to be replaced by a similar dipole from an adjacent vein. Moreover, if the second intermost vein is larger than the one nearest the surface, the dipoles released from them will also intersect the surface near the first extrusion. thus, for repeated cycling, dipoles will be translated from one cell to another with some of them reaching the surface. The total density of dislocations will not change, but the surface topography will. Actually, the dislocation dipole is translated to the surface (or other cell walls) during a small portion of the number of applied cycles since approximately 1000 dipoles correspond to a laminate of the extrusion and the number of cycles during this state is estimated to be about 10^6.

Basinski[6] reported that the surface defined by the array of dislocation cells does not necessarily lie parallel to the slip plane. This arrangement of dislocations in the interior of the crystal can lead to some of the surface features that were observed in the present experiments. Consider Figure 29 which is a section that contains a part of a dislocation cell lying near the surface. The plane of the array of dislocation cells is an an angle of α to the slip plane. During cyclic strain some dislocation dipoles are transferred from one cell wall to another. Those near the surface create extrusions or intrusions as has been indicated in Figure 28. In addition, dislocation pairs from veins farther from the surface will not be captured by the vein nearest the surface because of the tilt of the array of dislocation cells. Consequently, these dipoles will reach the surface and can form over lapping extrusions (or intrusions); this should give the appearance of a laminated extrusion as shown in Figure 29.

The braided appearance of the extrusions is dependent on the lateral positions of the dislocation sources. Consider the geometry of the dislocation

cell grid in Figure 30. If this grid is tilted as in the previous figure in addition to the sources being laterally displaced in a uniform manner, the extrusions will appear grouped as shown in Figure 30. If the surface is not well resolved possible because of oxide formation, a smooth braided appearance as seen in Figures 11b and 11d can result.

Because of the high stacking fault energy is copper, dislocations can readily cross slip, as a consequence, dislocation activity on this slip system can alter the extrusions. The effect is illustrated in Figure 31a. If the primary slip system is $(11\bar{1})$ [101], the cross slip plane is $(1\bar{1}\bar{1})$. Deformation in the [101] direction will only create steps on the ridge of the extrusion if the extrusion has a uniform cross section. The surface of the extrustion, which is the primary slip plane, will not be affected. A similar geometry of the extrusion will occur when the Burgers vectors of dislocations in other secondary systems is in the $[1\bar{1}0]$ or [011] directions. These dislocations can be active in regions where local stress fields due to grains of other stress modulators are present. If, however, slip occurs on planes in other slip directions, the $(11\bar{1})$ surface of the extrusion will be stepped as shown in Figure 31b. Both conditions are shown in the SEM photomicrographs and results in the fine structure especially noted in specimens fatigued in high vacuum.

Although the general features of the surface topography developed during fatigue in oxygen are similar to those observed in a vacuum, some decernable differences were noted. The lack of fine structure in the extrusion seems to be associated with the oxide formation during the development of new surface in the fatigue process. The fact that the intrusion-extrusion patterns are not grossly different in both cases, supports the claim that the atmosphere is not a controlling factor in crack nucleation as proposed by Broom and Nicholson[8], but is likely to affect the crack growth by altering the mechanism of blunting of the crack tip (Sumsion[9], Williams and Nelson[10]) or by corrosive type attack (Bradshaw and Wheeler[11]). Moreover, the lack of fine structure of the extrusions indicates that due to the oxide layer the egress or initiation of dislocations are impeded (Koehler[12], Head[13], Grosskreutz and Bowles[14]).

The thin layer of solute near the specimen surfaces change the character of the material considerably. In addition to longer fatigue life[15], the surface

solute layer generally prevented the nucleation and egress of dislocations. Only a few slip striations were noted; these, however, usually contained extrusions. These slip striations were found to be associated with the direction the fracture travelled. Treating the surface with a small amount of solute increased the critical resolved shear stress of the surface crust and impeded plastic deformation. The crust deformed only after the local stresses below the layer reached a critical level. It is expected that dislocations accumulated below the affected crust during fatigue established a region of high residual stress. The large extrusions which were seen below this surface must have been produced at the time of fracture when this residual stress was somewhat relieved. The magnitude of the extrusions must reflect the accumulated dislocation debris under the layer.

The increase in the critical resolved shear stress of the crust can be due to the development of accommodation dislocations or solute hardening as shown by recent work on the copper-gold system.[16]

4. Conclusion

Environment and thin-diffused coating are quite effective in influencing the fatigue characteristics of copper crystals. In uncoated crystals, dipole and multiple arrangements of dislocations are basic to the mechanism of extrusion-intrusion formation; environment can effect the fine structure. The fine structure that will produce sharper notches in the surface does not lead to early fatigue failure; instead, the more uniform structure which is formed in oxygen atmosphere is associated with shorter life. Thus, it is expected that a blunting mechanism or corrosion attack control the progress of the crack.

The extrusions and intrusions are produced by dislocations from the cells; consequently, there is a relationship between the surface markings and the internal structure. The extrusion is elongated in the direction of the Burgers vector of the primary slip system. Secondary slip is also noted but in general it only modulates the primary patterns.

Diffusion layers result in a crust that has a higher yield strength than the bulk material. These layers greatly limit the dislocation activity at the surface. Below the crust, however, a residual stress is produced because of a heavy concentration of dislocations. Upon fracture these dislocations are relaxed by forming extrusions and intrusions directly under the crust on the fracture surface.

PART III COMPARISION OF THE MECHANICAL PROPERTIES OF DIFFUSION COATED AND UNCOATED CRYSTALS

The rate of work hardening and the hysteresis energy loss during fatigue were measured. As described in Part I, the specimens used were tapered cantilever single crystals. Generally, the displacement of the narrow end was $\pm$ 1.0mm during the cycling; this deflection produced a surface strain of about 5×10^{-4}.

The equipment, although designed and built in a relatively short time, produced fairly reproducible experimental data for most specimens.

Before a fatigue test could be run, the specimen was carefully arranged in the grips of the fatigue machine. To prevent initial deformation of the single crystals, the sensitivity of the electronic measuring equipment which indicated the load on the specimen and its position was increased from 10 to 100 times the value necessary for the actual test. Thus, the securing of a specimen in the grips was monitored and if the load or position was not correct a mechanical adjustment was made.

During the pump down of the environment chamber, care was taken to prevent loading of the specimen. When the proper environment was achieved, the specimen was deformed slowly, usually by manually rotating the shaft of the transmission. A plot of the load verses displacement was recorded on an X-Y recorder during the deformation. Usually, the first 100 cycles were produced in this way so that a complete record of the change in mechanical hysteresis and hardening rate was indicated on the read out devices. Figures 32a, 32b and 32c show a sequence of energy loss curves for specimen 18 - a crystal coated with a diffused layer of gold. Figure 32a is the first three cycles recorded at a setting of 0.5 volts for the X and Y channels. Figure 32b demonstrates the change in shape of the hysteresis curve up to N equal to 35 cycles; the amplification factors were altered in this recording to give more sensitivity. In Figure 32c, the most drastic changes in the area of the curves are noted; the energy loss decreased considerably in this range. All these hysteresis curves were produced by manually turning the shaft to the transmission since the pen speed of the X-Y recorder was quite slow. However, between recorded cycles, the specimen was cycled at about 35 cps by the sevomotor (see Part I).

At times it is convenient to record the load-displacement information on the oscilloscope. This is accomplished with a Polaroid camera, and examples of these results are shown in Figure 33. Since quantitative measurements can not be obtained by this method, this system was employed during the fast cycling to note dynamic hysteresis loops and to assist in making fine adjustments in the frequency. Figure 34 shows two resulting patterns for a 50 cps cycling rate. It should be noted that the loop is broader than found during the manual deformation. Apparently a secondary wave, probably from resonant conditions, modulates the original frequency. Thus, continuous recording is quite important since the system can be tuned to minimize this effect.

The average load applied to the beam was recorded continuously. This plot indicates the change in hardness level during the test and gives a direct reading of work hardening rate. Also it indicates the rate of decrease in load when a crack propagates through the crystal. Results derived from these data is shown in Figure 35. The two specimens compared are No. 14, no coating, and No. 18, diffusion coated. The diffusion coated specimen deforms at a higher initial load than the untreated crystals. Moreover, the rate of cyclic hardening is greater for the surface treated specimen. At about 10^5 cycles - an accumulative strain of 500% - both untreated and treated crystals tend to act similarly because the hardening rate has decreased to zero.

Somewhat similar results are seen in the curves of energy verses number of cycles. These data are plotted in Figure 36. The energy loss in those crystals not coated with a diffused layer of gold increases very slightly over the first 10 cycles, grows to a maximum at about 10% accumulative strain, decreases and reaches a constant value at 400% strain at 5×10^3 cycles. On the other hand, the energy loss of the gold treated specimen increases more rapidly from the start, peaks at 3.5% accumulative strain and decreases to a value of energy loss similar to the constant value attained by the uncoated crystals. This level seems to be reached after about 250% accumulative strain. Comparison of the curves shows that the coated crystal has at 15% greater energy loss than the untreated crystals.

Discussion of Results:

The apparent difference in the work hardening and the energy loss curves should be a result of a variation in deformation mechanism. However, care must be taken in interpreting these results since more data is necessary in order to make firmer conclusions.

A number of experimental facts have indicated that diffused coatings alter the mechanical properties of single crystals. Many of these were discussed in Part II of this report. For example, surface striations and the fracture characteristics near the surface are grossly altered by diffusion coatings. Fatigue life is changed, and in the case of gold on copper, the lifetime is increased. Other experiments have shown that the critical-resolved shear stress is increased by compositional changes at the surface. All this evidence and the data obtained in this portion of the experiments point to the fact that small changes in surface conditions affect the dislocation nucleation, movement and multiplication. The difference in yield stress in bending and the increased rate of work hardening for the surface treated crystals indicate that the effects are long ranged. The significant change in energy loss relationship also relates to this condition. It is believed that the initial build up of dislocation density, especially near the surface, is greater in the coated crystals. This can lead to a greater rate of increase of work hardening; and, consequently, higher energy losses at lower accumulated strains. The maxima which occur in these constant total strain amplitude cycling experiments are a result of the increasing ratio of elastic strain energy to plastic strain energy as the number of cycles is increased. This effect should be characteristic of a soft material that work hardens considerably during cyclic straining. Nevertheless, the displacement of the maxima is significant.

This work has uncovered several effects which indicate that the mechanical properties of diffusion coated materials can be optimized by using the correct combination of treatments and materials. However, it is important to understand more of the basic principles of surface hardening. Still required are studies of the problems of crack development and propagation for different surface conditions and environments. Part II of this report demonstrated that fine structure

of the striations produced by fatigue is related to the environment. Although it appears that nucleation of the crack is independent of the environment, it is still necessary to consider this effect for materials other than copper. Moreover, the dependence of surface hardening on stacking fault energy changes, solute hardening, accommodation dislocations, etc. must be better understood.

The technical usefulness of coatings on material have been demonstrated for many years. With the recent advances in the understanding of the ralationship between strength of materials and structures, it is the proper time to attempt to apply some of these principles to the problems of surfaces.

REFERENCES

1. Cottrell, A. H. and Hull, D., Proc. Roy. Soc., 242, 211 (1957).

2 Forsyth, P.J.E., J. Inst. of Metals, 80, 181 (1951-52)

3. Schiejve J. "Analysis of the Fatigue Phenomen in Aluminum Alloys", T.R.M 2122, National Lucht-en Ruimtevaart-Laboratories, Amsterdam, (1964).

4. Laufer, E. E., and Roberts, W.N., Phil. Mag., 10, 883 (1964).

5. Lukas, P.and Klesnil, M., Physica Status Solidi, 21 ,717 (1967).

6. Basinski, S.J., Basinski Z.S. and Howie, A., Phil. Mag. 19, 899 (1969).

7. Chen, H. S., Gilman J. J., and Head, A.K., J. Appl. Phys., 35, 2502 (1964).

8. Broom, T., and Nicholson, A. Jour. Inst. of Metals, 89, 183 (1960-61).

9. Sumsion, H.T., J. Spacecraft, 5, 700 (1968).

10. Nelson, H.G. and Williams D.P., NASA Ames Report, "The Effect of Vacuum on Various Mechanical Properties of Magnesium", also Williams, D.P. and Nelson H.G., Trans AIME, 233,1339 (1964).

11. Bradshaw, F.J., and Wheeler, C., Inter. Journal of of Fracture Mechanics, 5, 255 (1969), and Applied Mat. Res., 5, 112 (1966).

12. Koehler, J.S., Phys. Rev., 60,397 (1941).

13. Head, A.K., Phil. Mag., 44, 92 (1953).

14. Grosskreutz, J.C. and Bowles, C.Q., "Environment Sensitive Mechanical Properties", (Gordon & Breach, 1965)

15. Dover, W.D., and Jones, W.J.D., Brit. J. Appl. Phys., 2,669 (1969).

16. Dejonghe, L.C., and Greenfield, I.G., Acta Metallurgica,1411 (1969); Patterson, W. Ph.D. Dissertation, 1969.

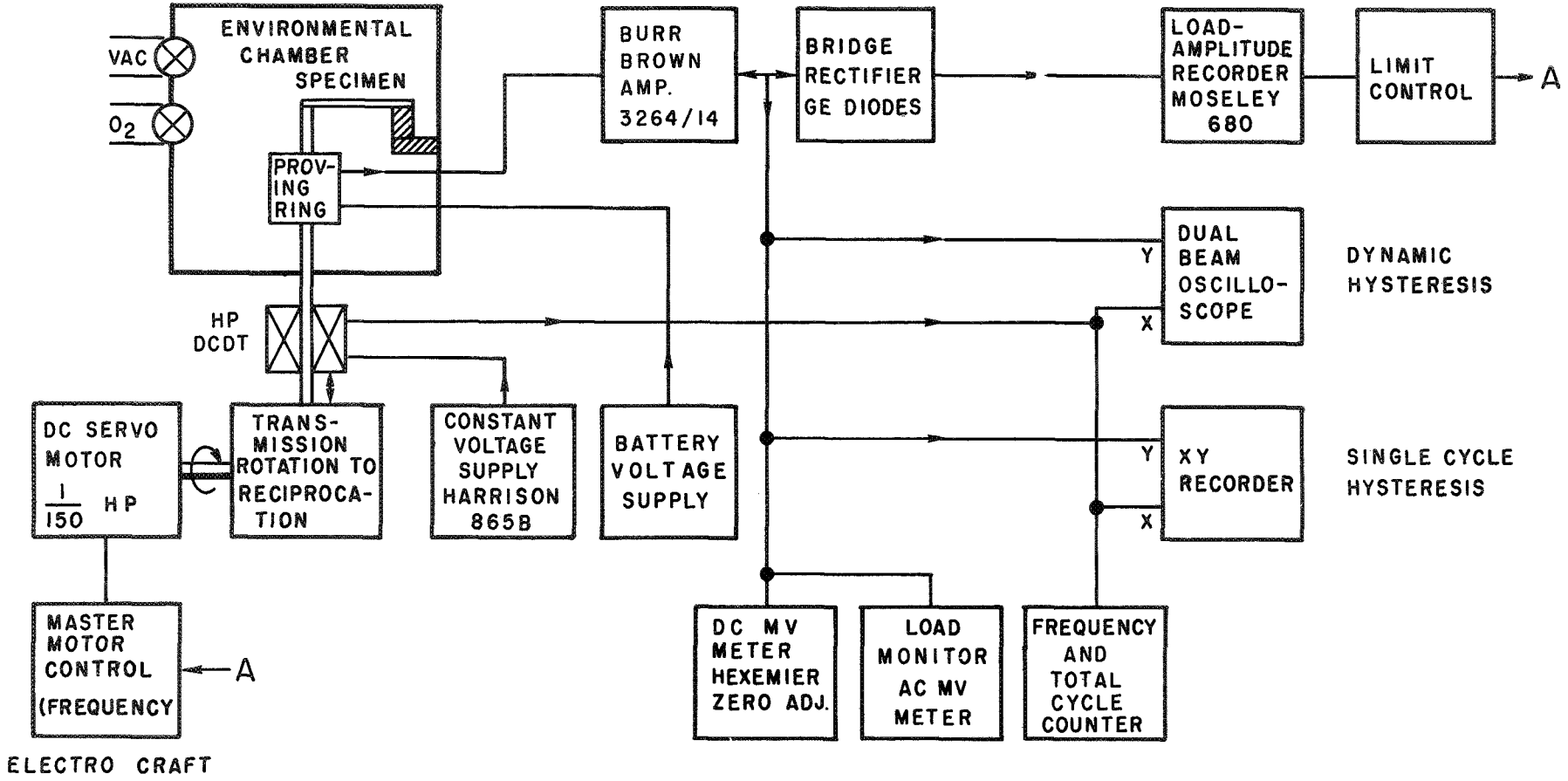

BLOCK DIAGRAM FATIGUE MACHINE

Figure 1. Block diagram of fatigue machine.

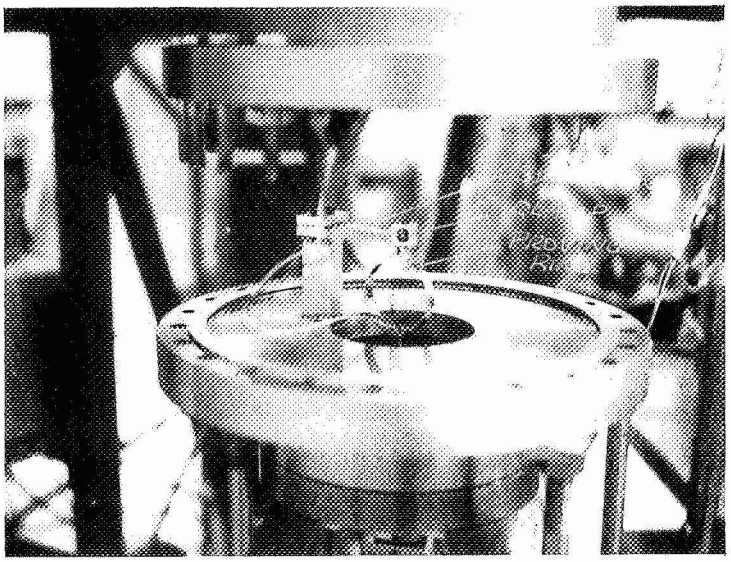

Figure 2. Specimen chamber.

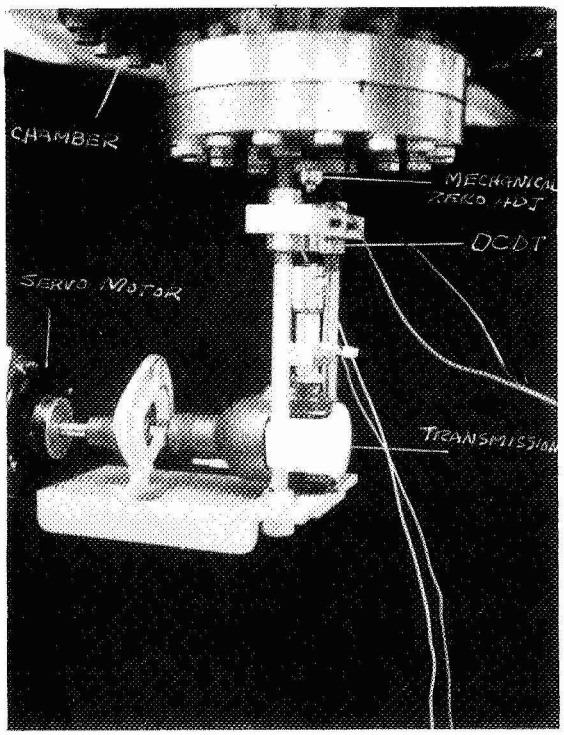

Figure 3. Transmission and construction details.

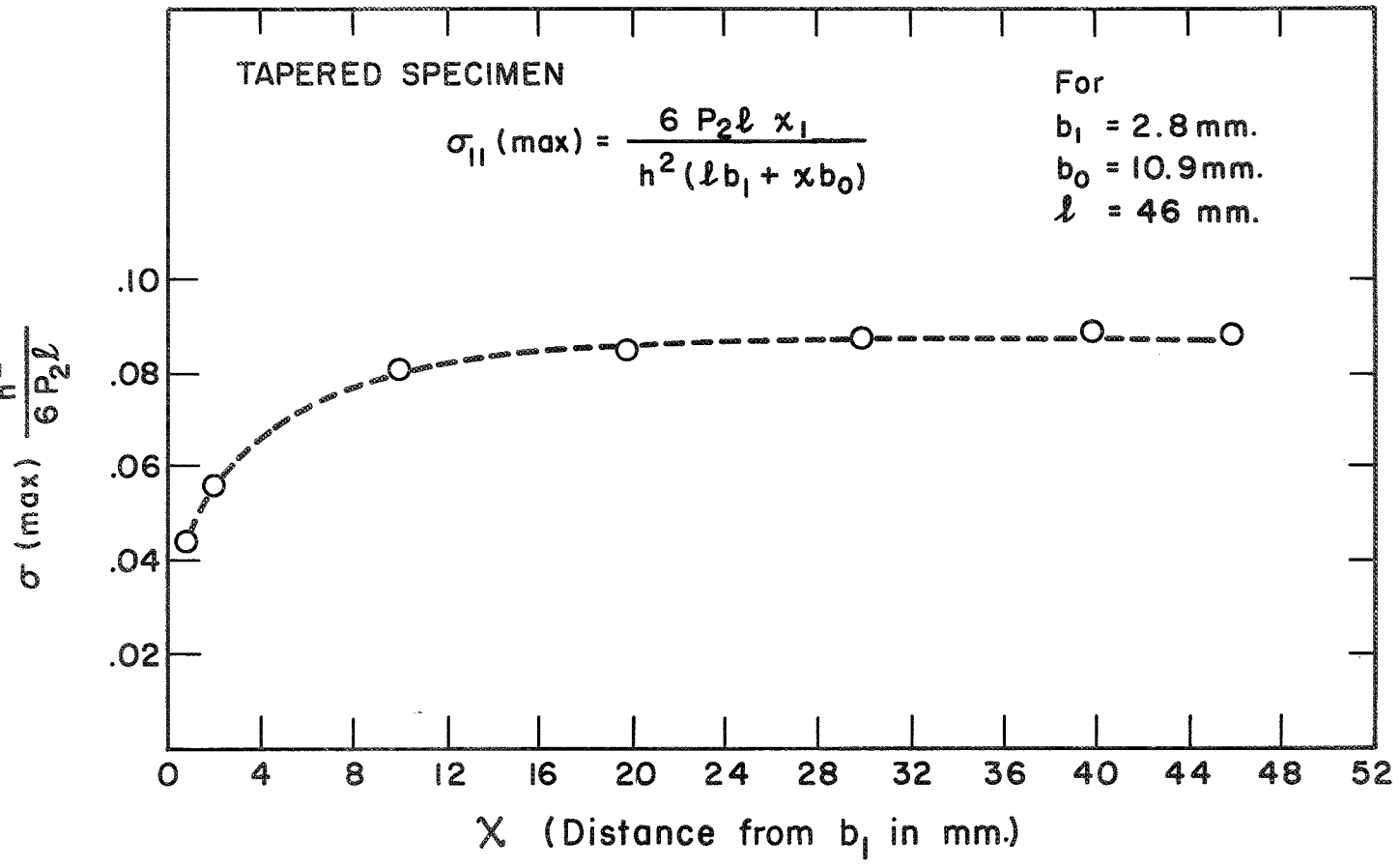

Figure 4. Plot of stress vs. distance along specimen for tapered specimens.

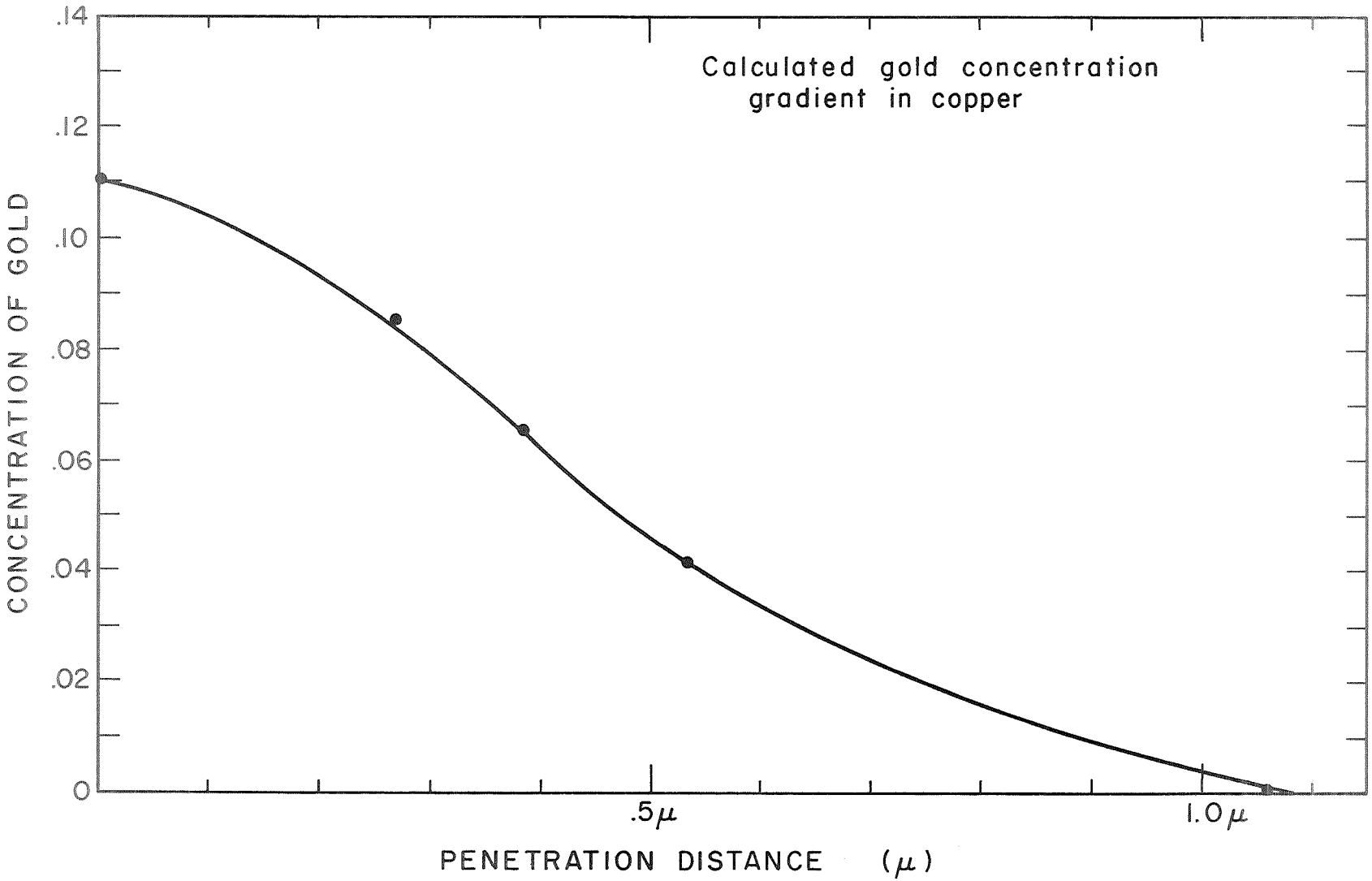

Figure 5. Penetration curve of Au in Cu.

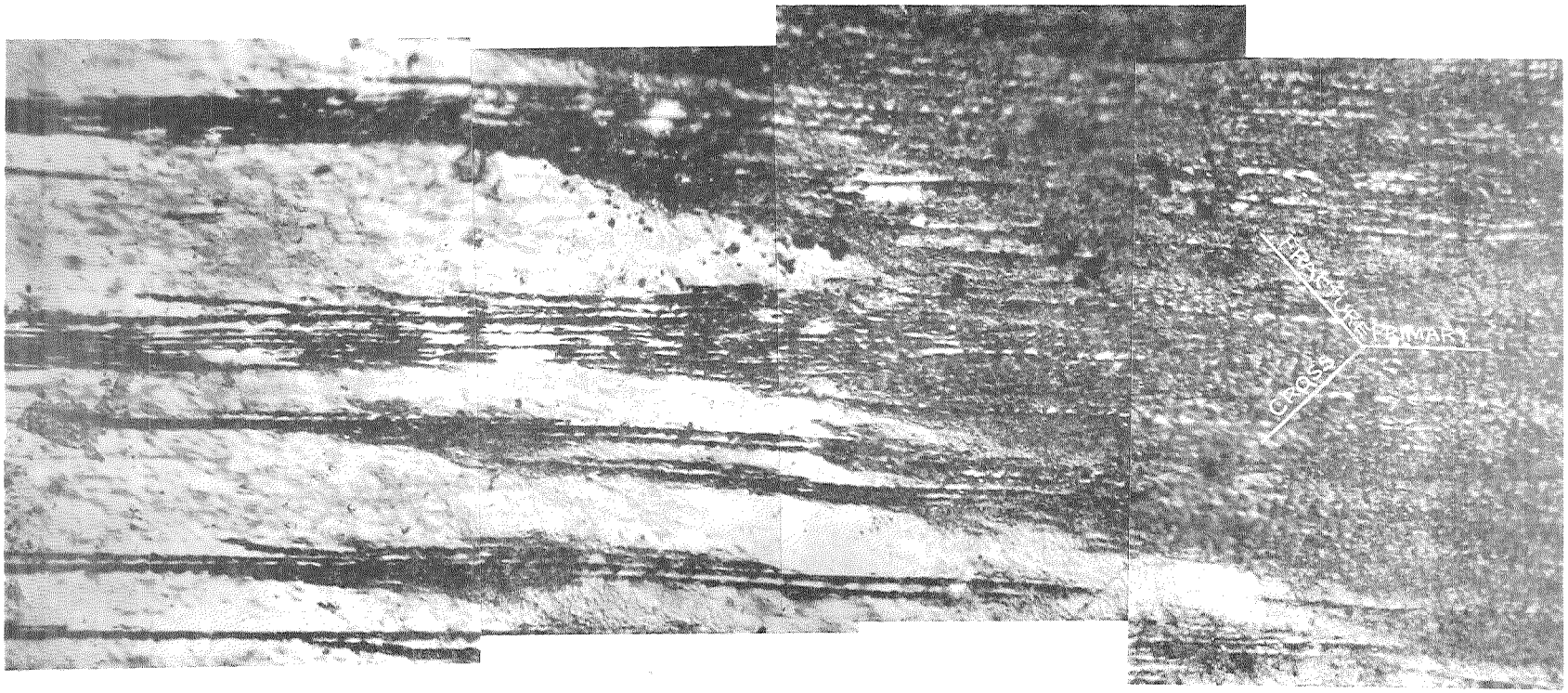

Figure 6. Optical photomicrographs of the specimen surface near the fracture; intersections of primary plane, cross slip plane and fracture surface are indicated; density of striations decreases rapidly at a short distance from the fracture; Specimen 12; X 500.

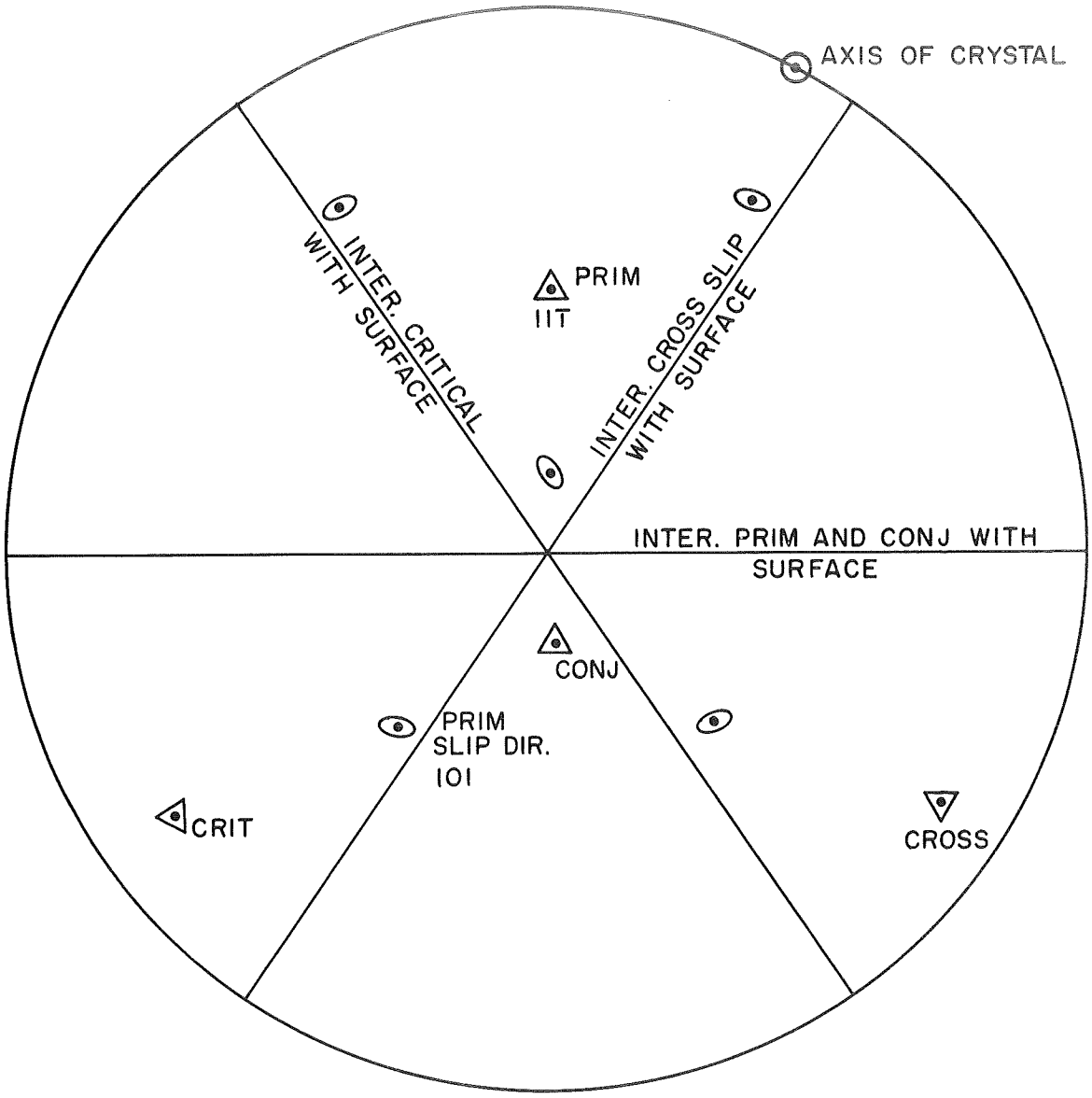

Figure 7. Orientation of Specimen 12.

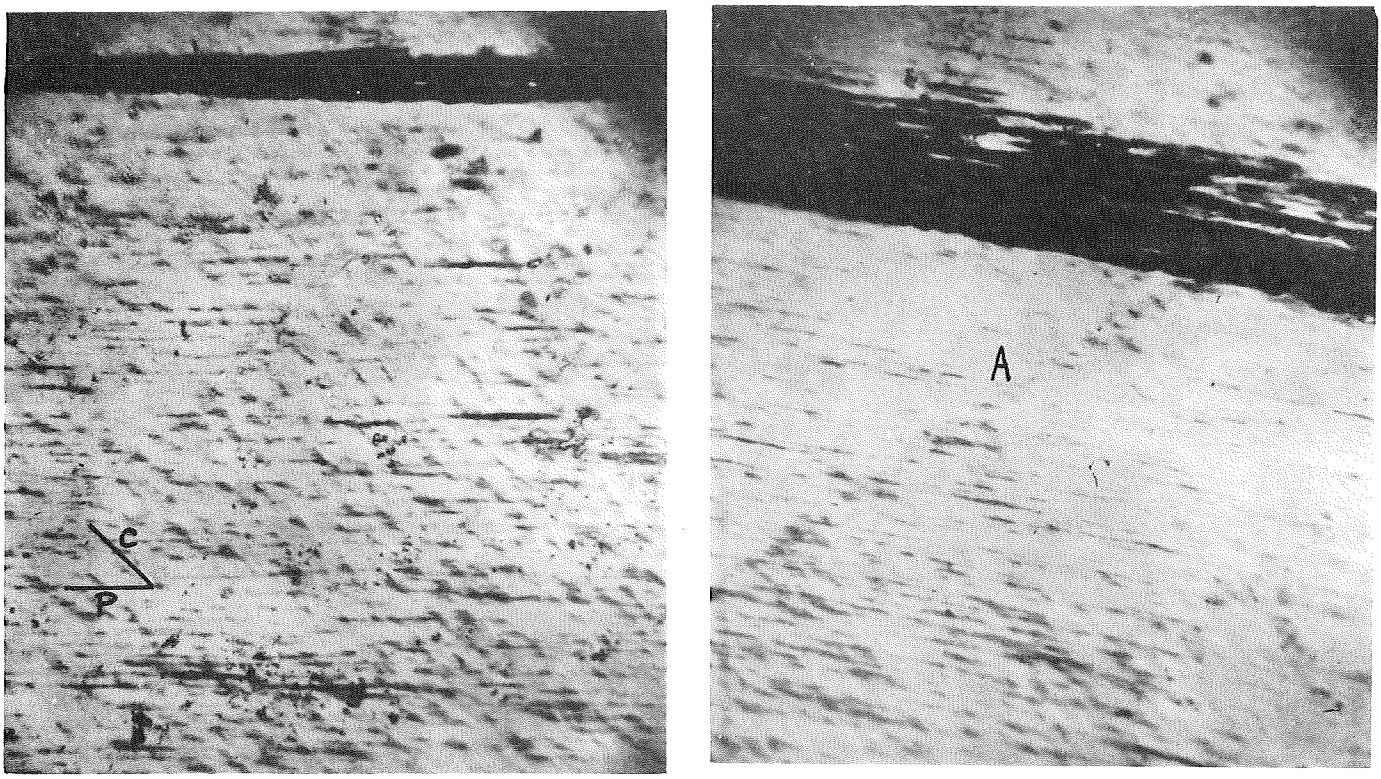

Figure 8. (a) Serrated slip lines between clusters; primary and cross slip systems are observable;
(b) Serrations aligned along the critical slip system at A.

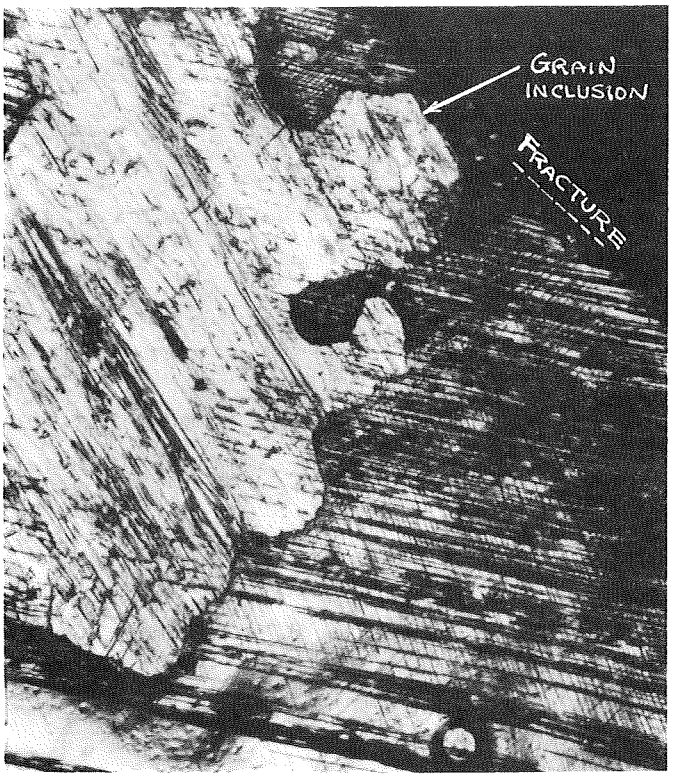

Figure 9. Small grain inclusion in crystal; note many slip systems acting.

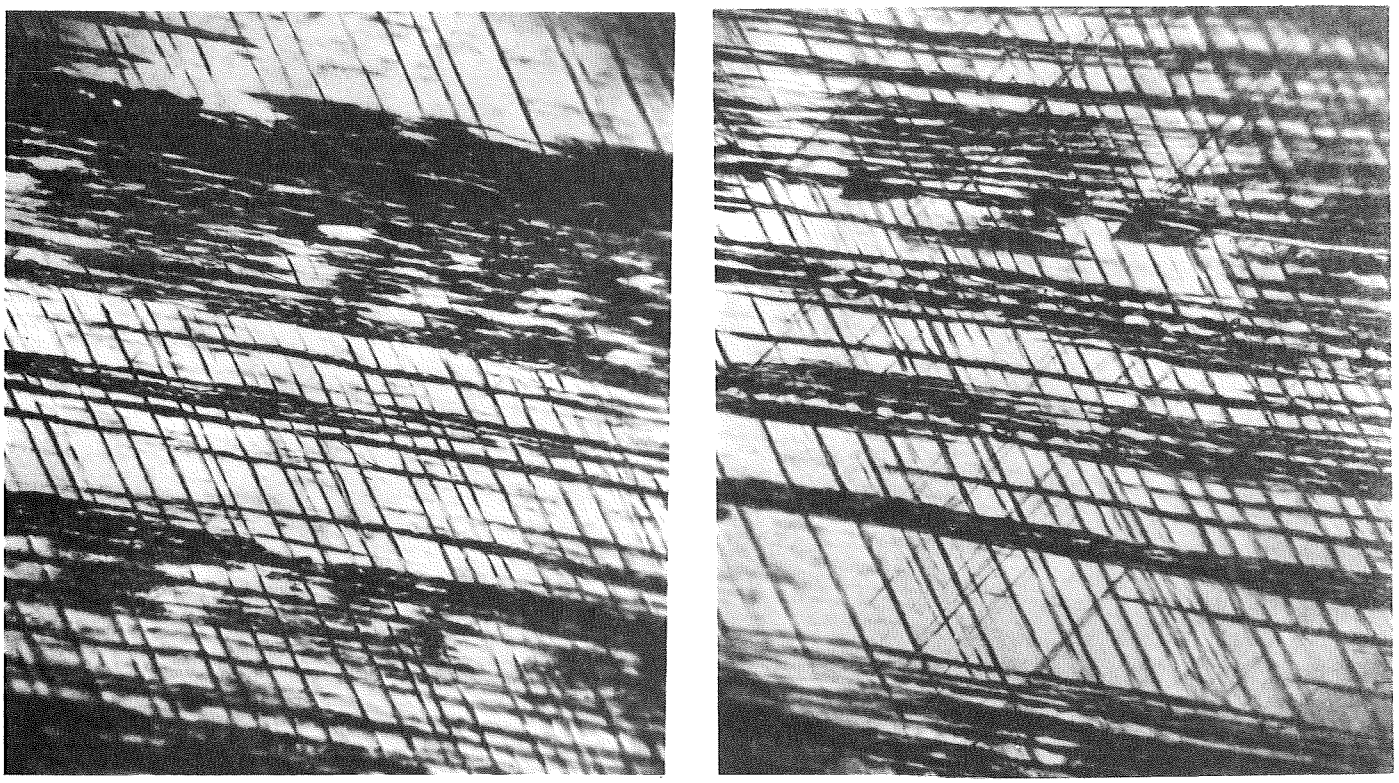

Figure 10. (a) primary and cross slip plane activity.

(b) primary, cross and critical slip planes active.

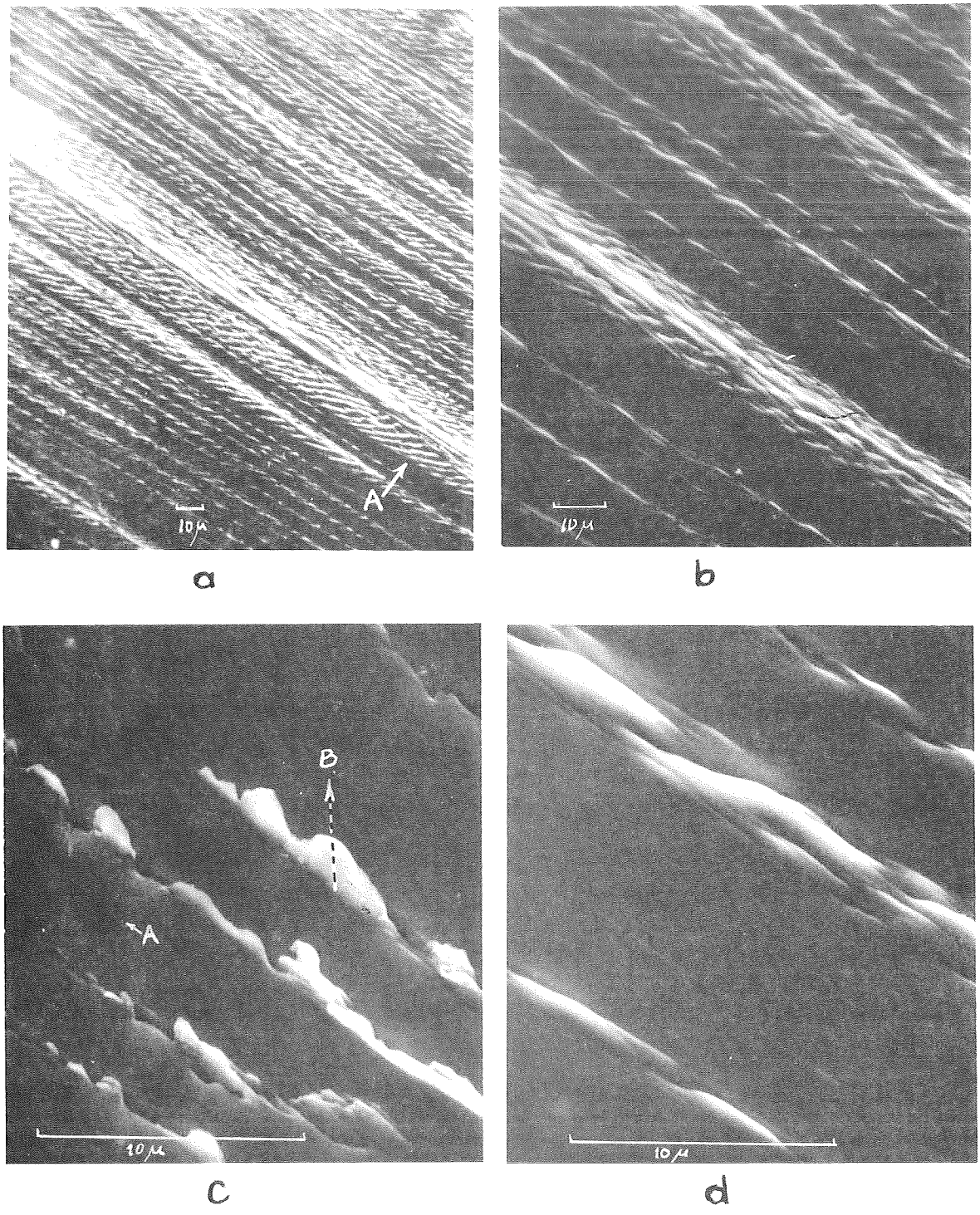

Figure 11. (a) SEM striations; Specimen 12

(b) braided appearance of clusters of striations;

(c) extrusions A cross slip, B is the Burgers vector;

(d) higher magnification of braided structure.

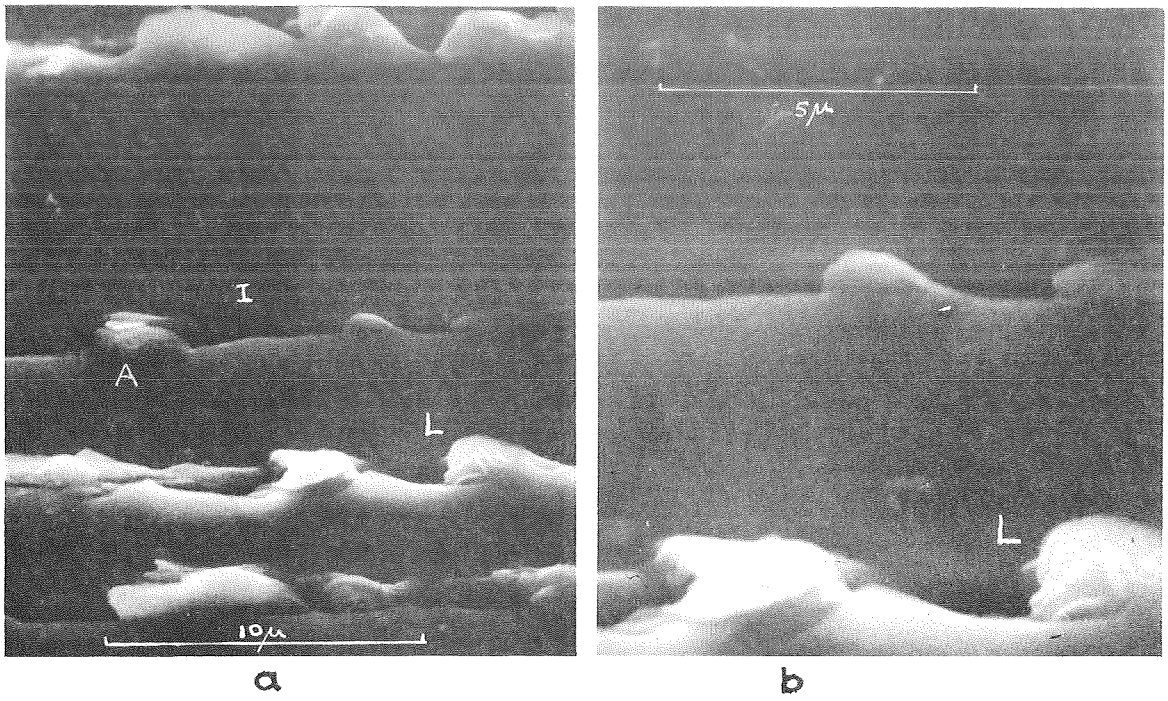

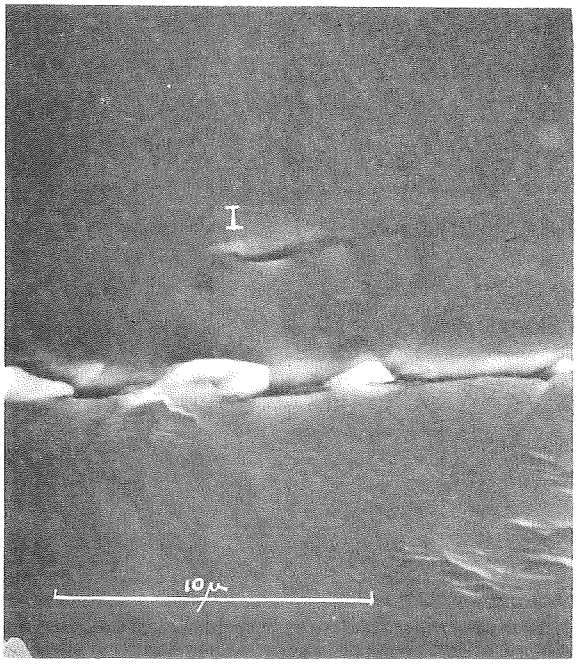

Figure 12. (a) Intrusion valleys and extrusions; extrusion A and L are laminate-like.

(b) higher magnification of extrusion L

(c) short intrusion at I

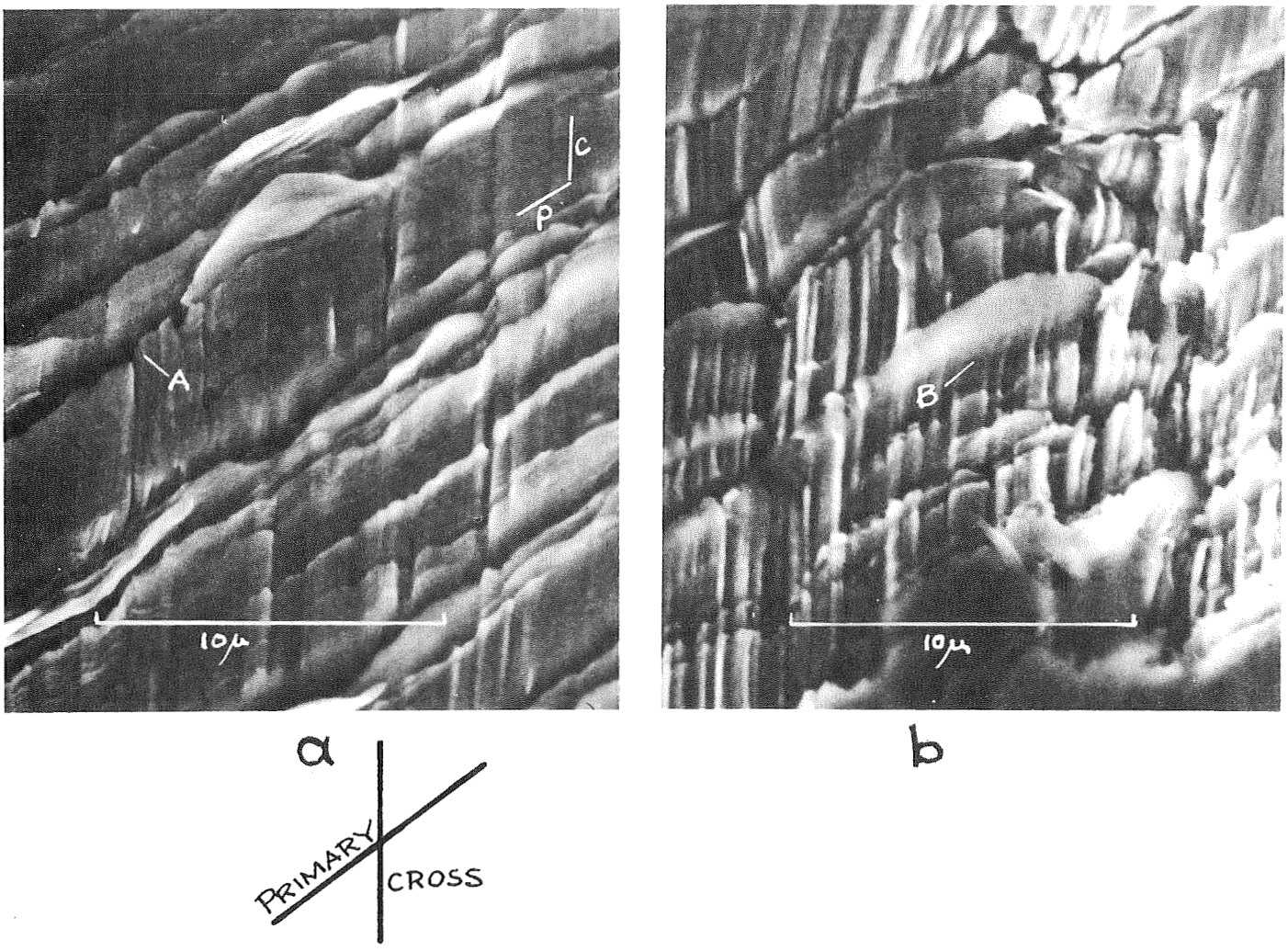

Figure 13. (a) Large extrusions on primary slip system and deformation on the cross slip system; the effect of combined primary and cross slip is shown at A

(b) lack of cross slip in a primary extrusion, B

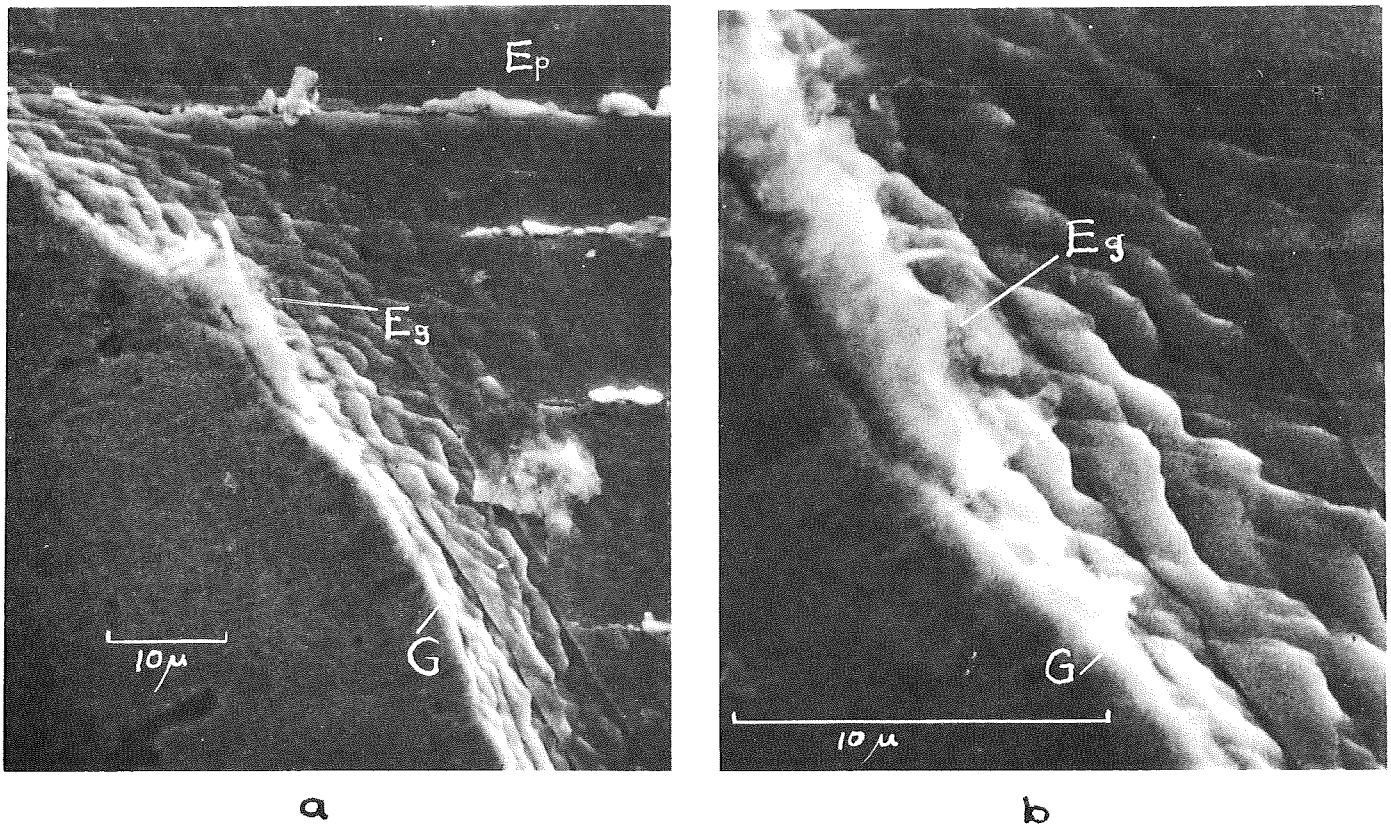

Figure 14. (a) Extrusion at a grain boundary; G is the grain boundary extrusion, Ep is an extrusion on the primary system

(b) higher magnification of Eg.

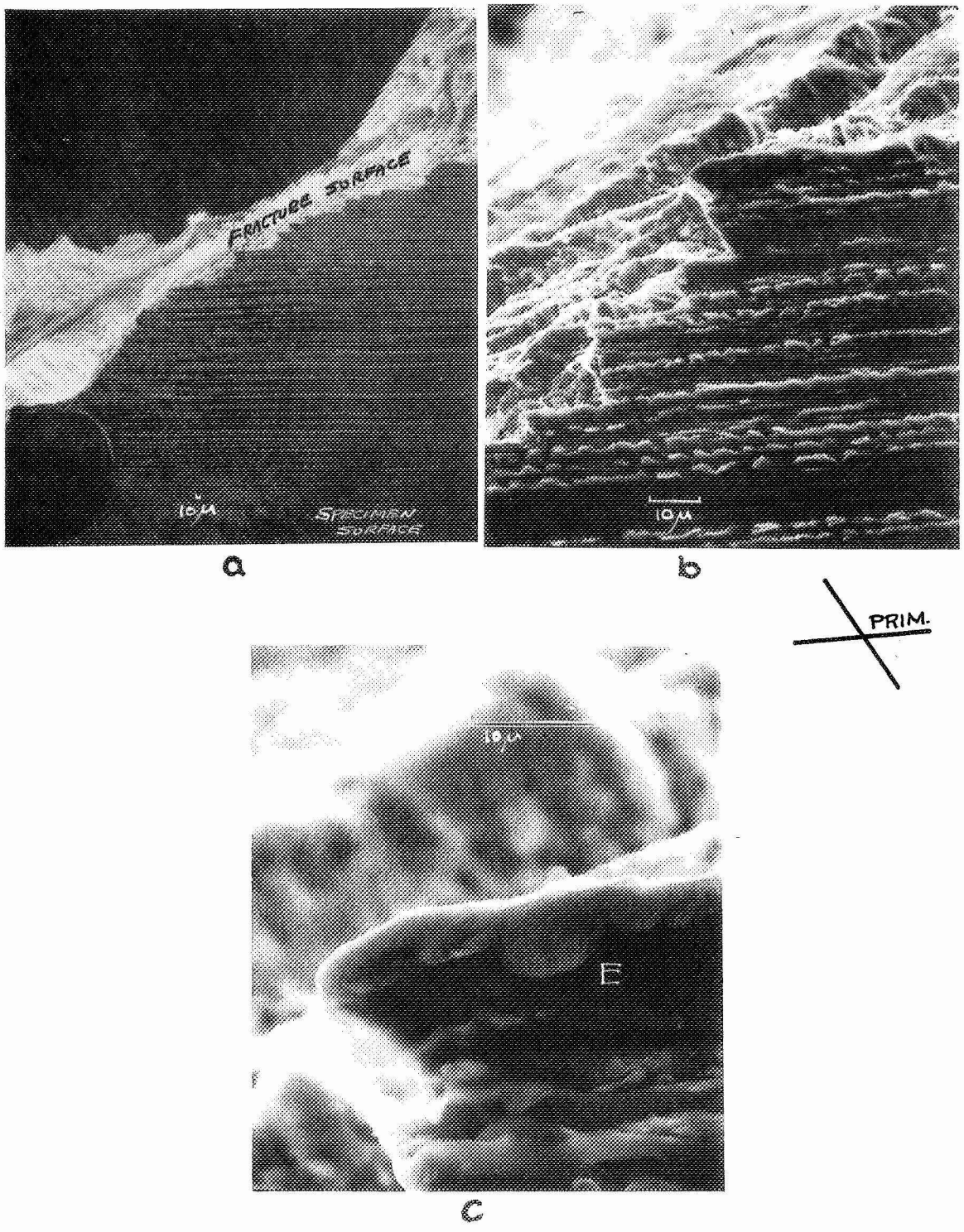

Figure 15. (a) Primary slip serrations and fracture surface

(b) fracture surface along primary and cross slip planes

(c) detail of extrusion, E, on fracture surface.

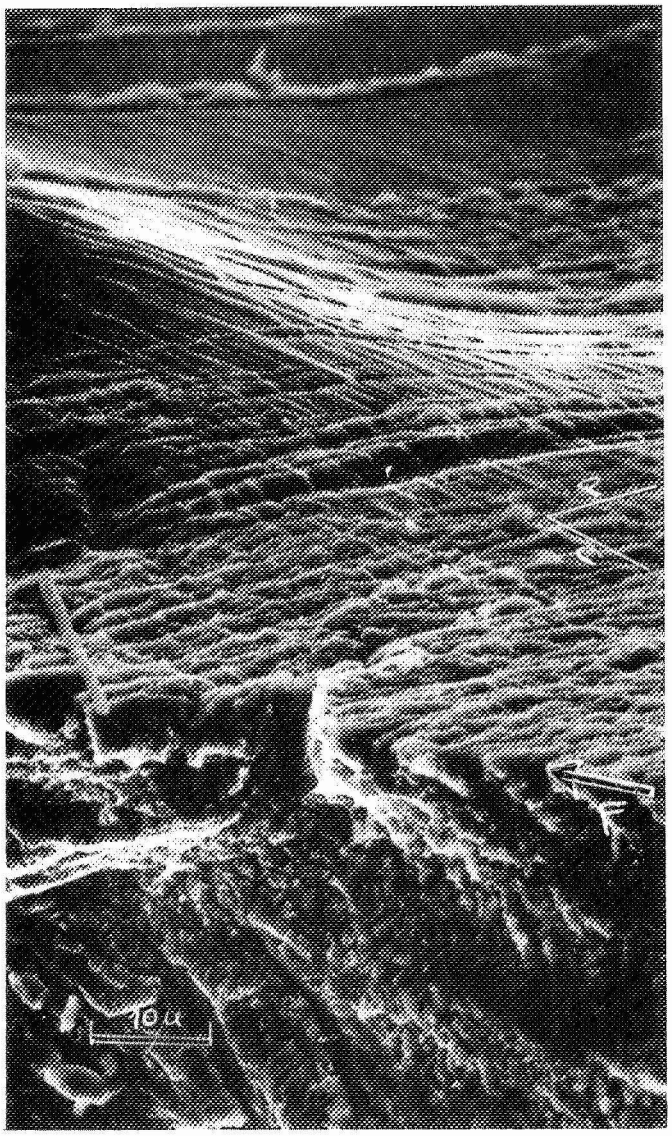

Figure 16. Intersection between the fracture surface and the specimen surface; primary slip extrusion and cross slip extrusions are visible.

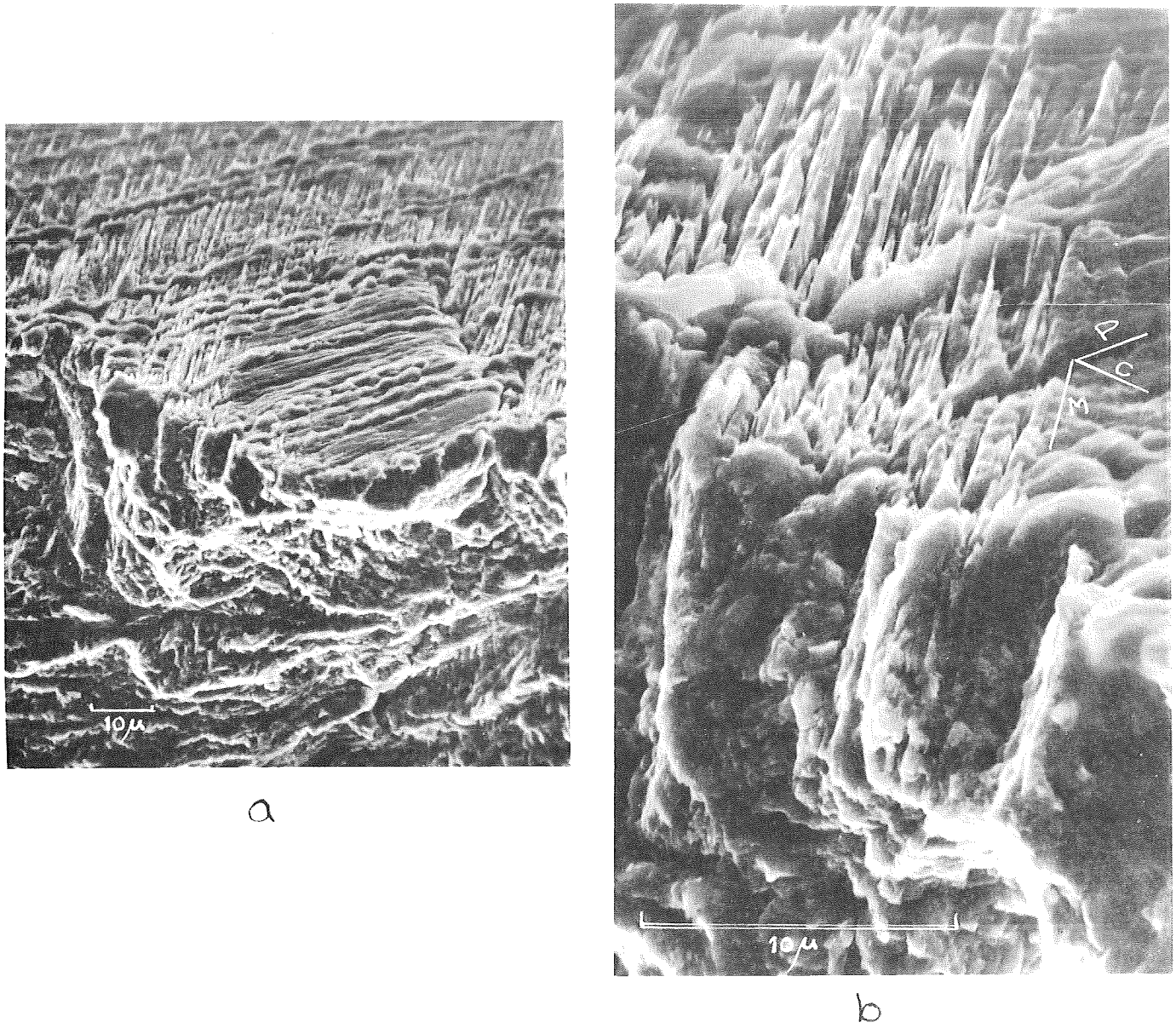

Figure 17. Intersection between fracture surface and specimen surface.

(a) Primary slip system P and critical slip system M are seen

(b) large extrusion extending 5u into the fracture surface are visible.

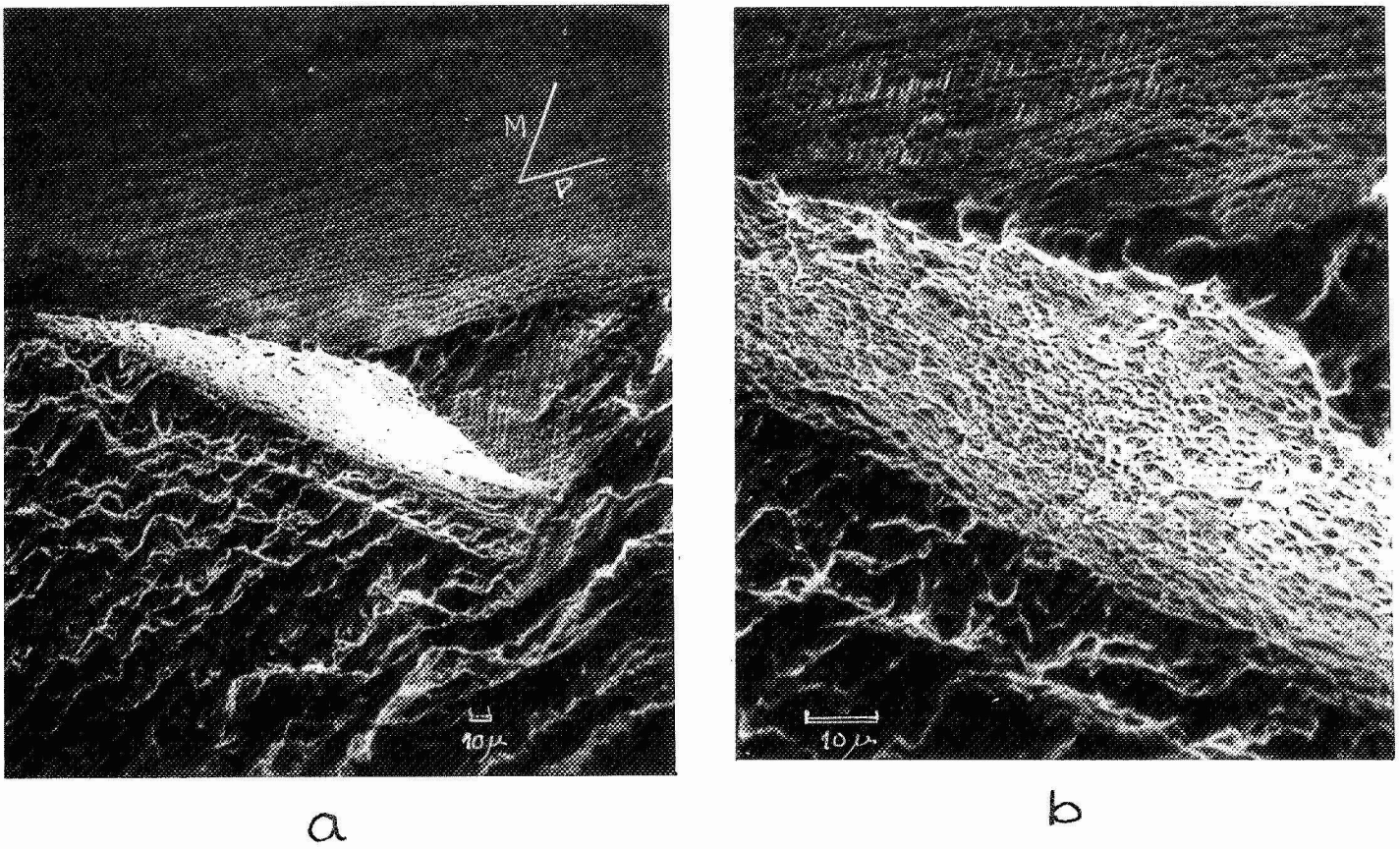

Figure 18. (a) Fracture along primary and a secondary slip planes

(b) detail of above

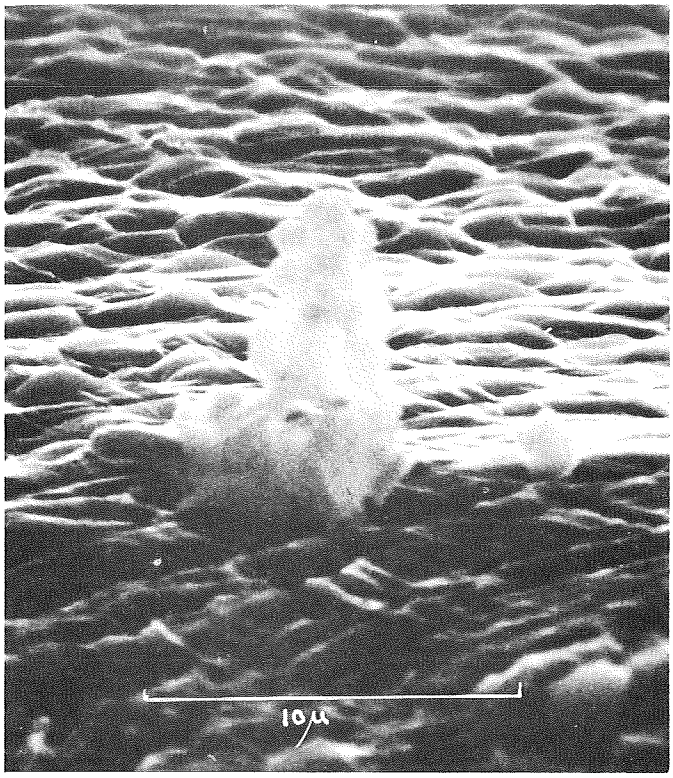

Figure 19. Large extrusion on specimen surface.

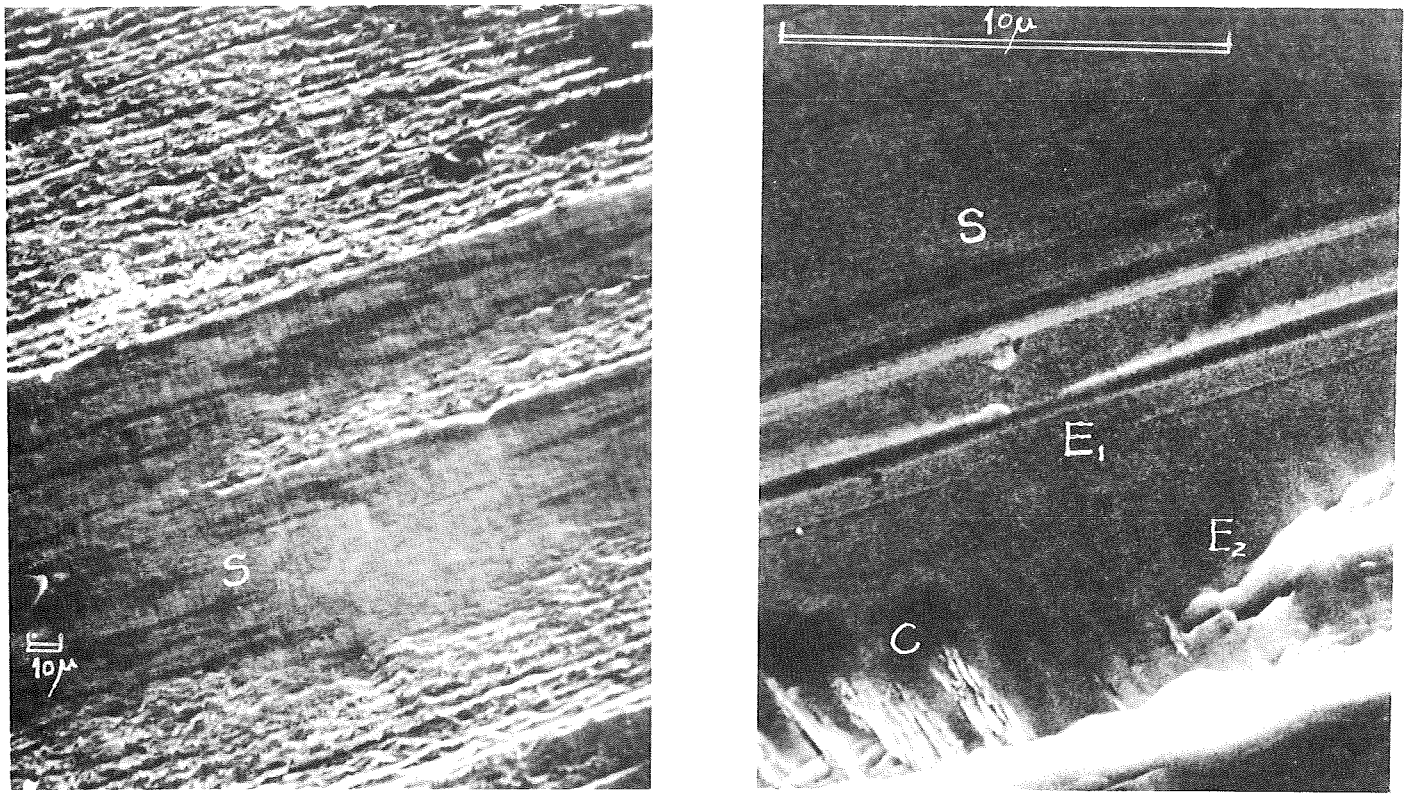

Figure 20. Specimen 14, fatigued vacuum of 10^{-7} toor.

(a) Low magnification; fatigue striations and slip lines, S.

(b) another region at higher magnification.

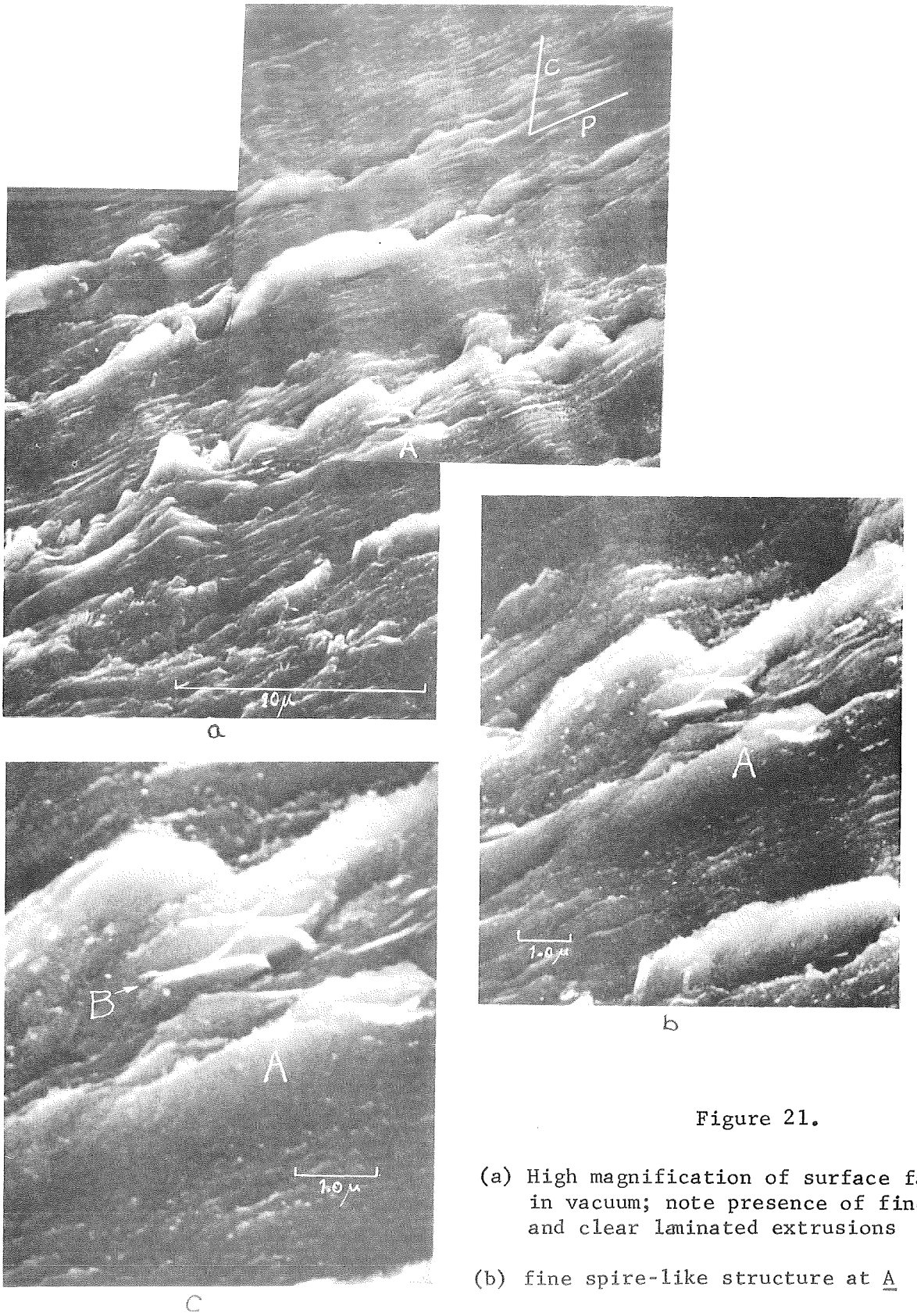

Figure 21.

(a) High magnification of surface fatigued in vacuum; note presence of fine structure and clear laminated extrusions

(b) fine spire-like structure at A

(c) clear laminates at B.

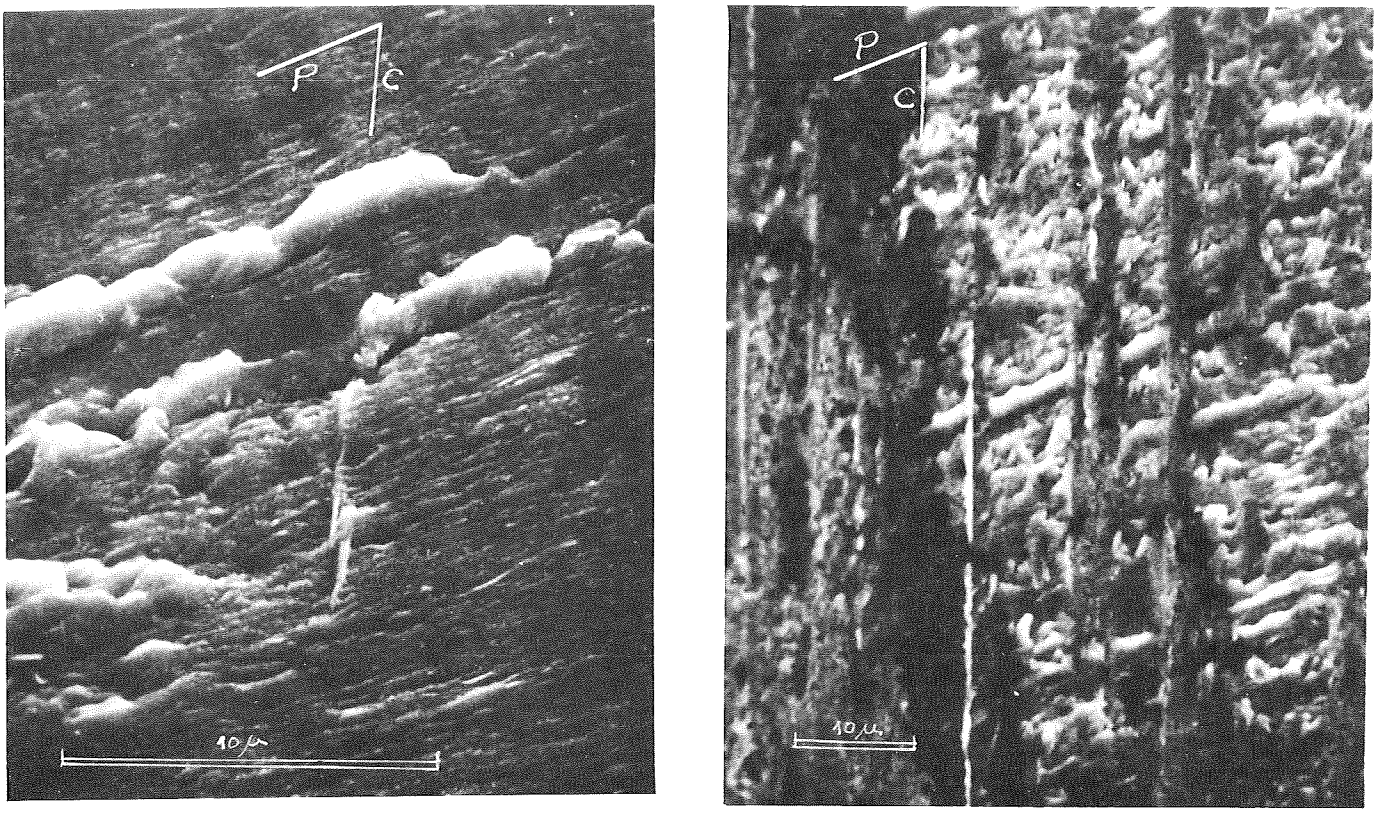

Figure 22. (a) and (b) comparison of cross slip in two regions of the specimen.

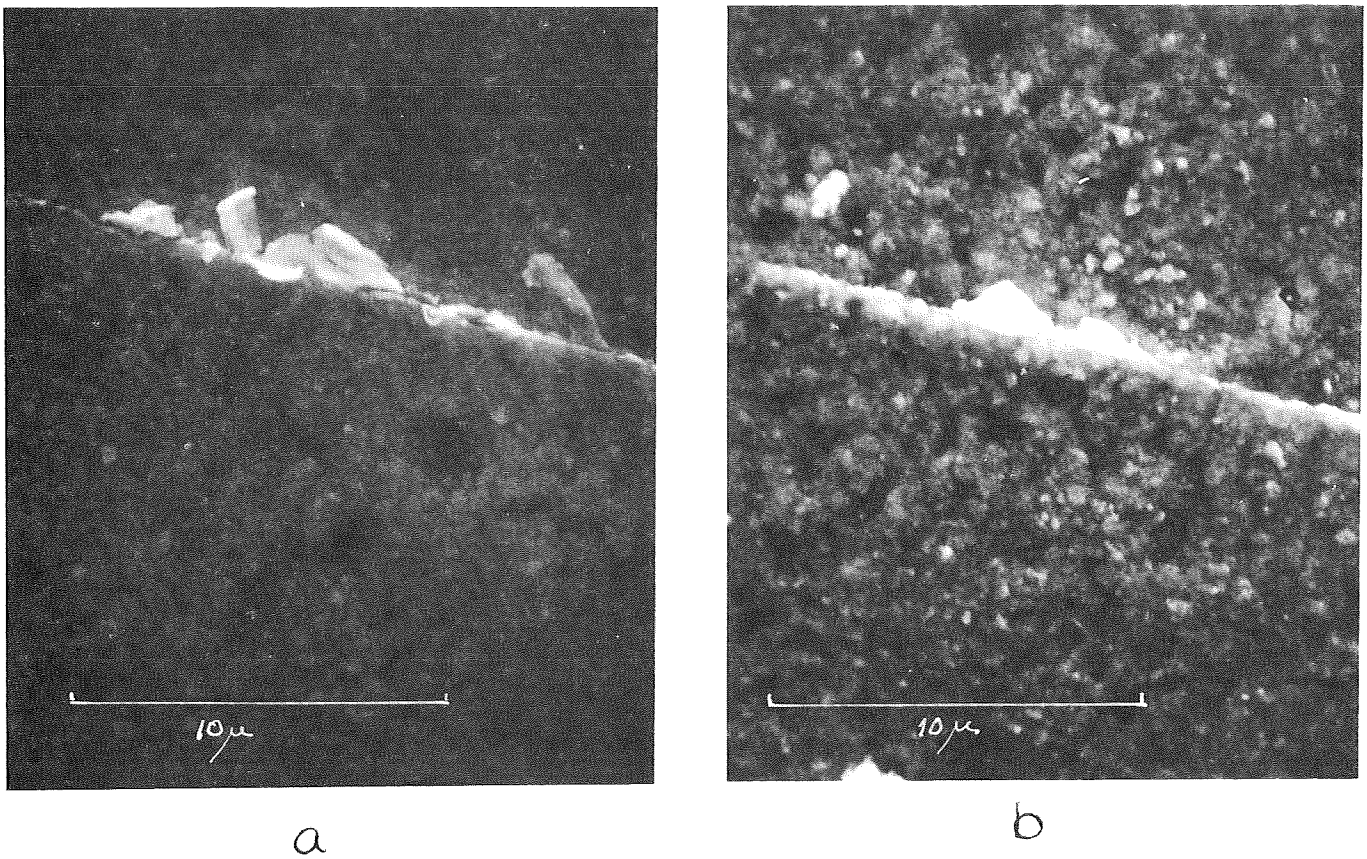

Figure 23. Copper crystal with a gold diffusion layer. (a) and (b) show very few striations; extrusions are visible also.

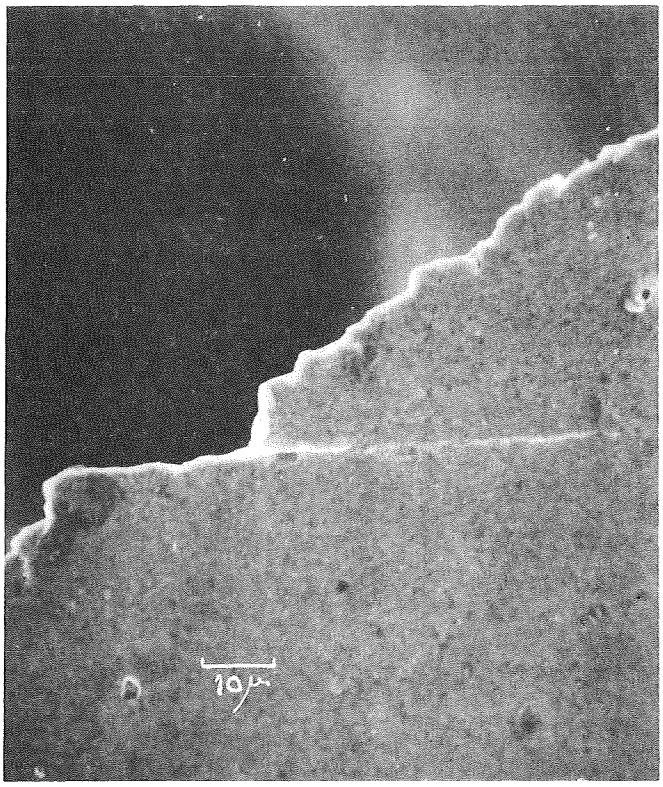

Figure 24. Fracture edge of coated crystal.

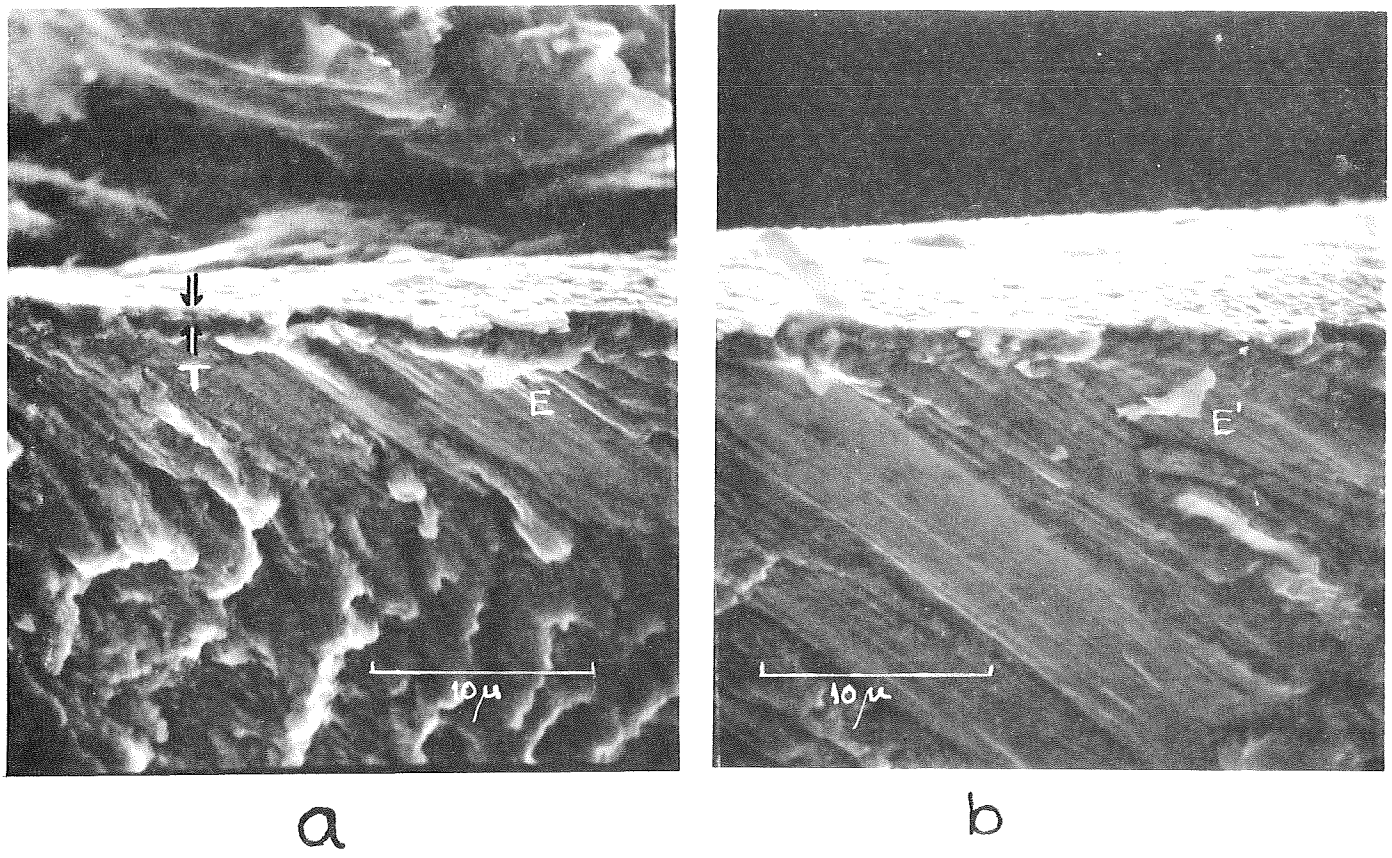

Figure 25. Fracture surface of coated crystal
(a) Crust like formation at T, extrusion extending from below crust

(b) Extrusion in fracture surface

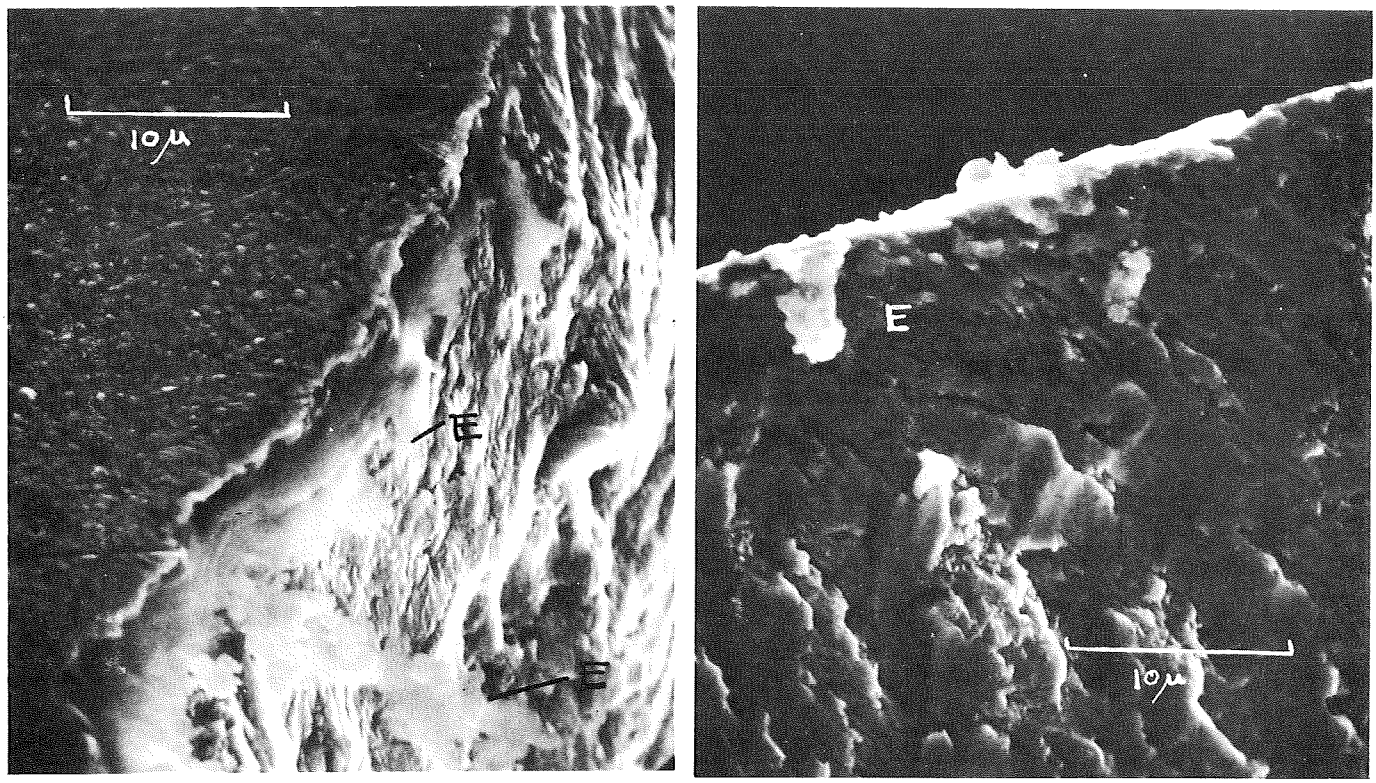

Figure 26. (a) and (b) extrusions from below crust.

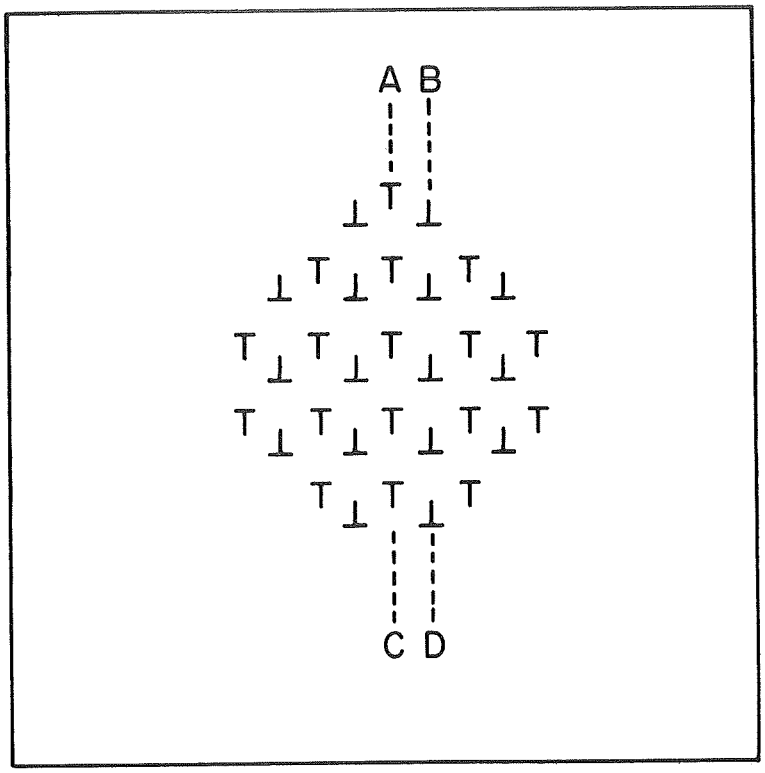

Figure 27. Cross section of a cell wall (vein).

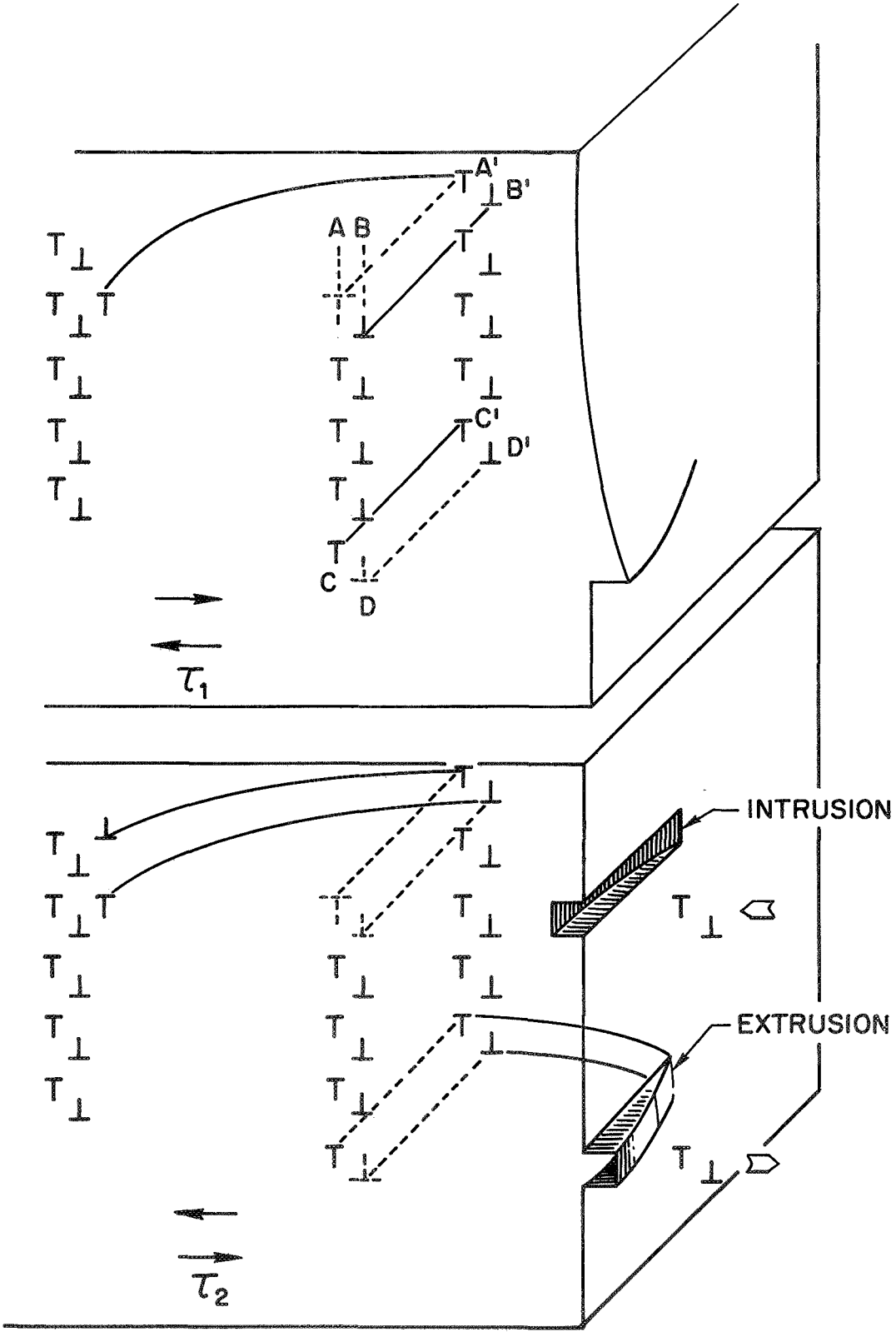

Figure 28. Movement of diploes in cyclic straining.

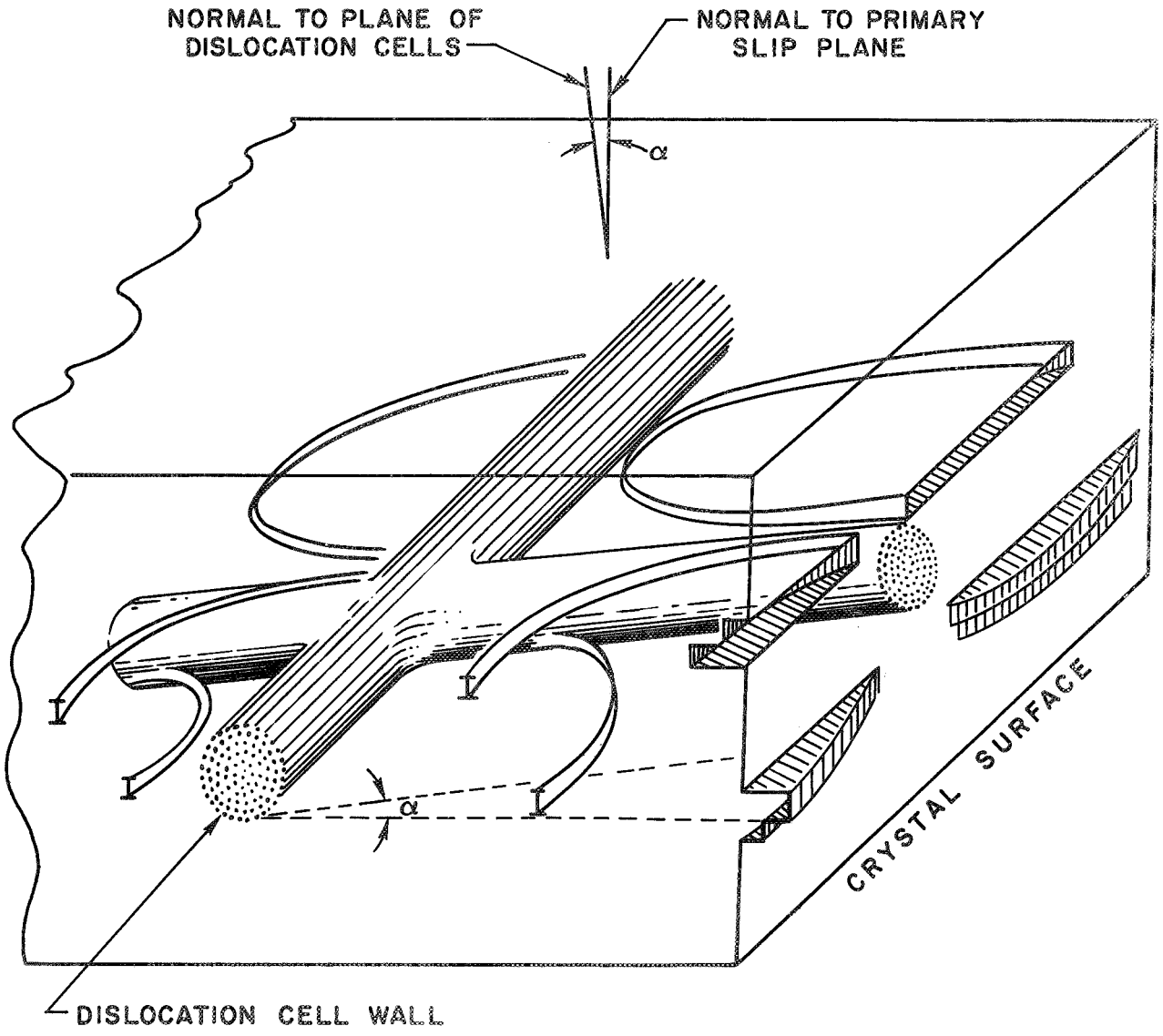

Figure 29. Detail of dislocation action forming laminated extrusions.

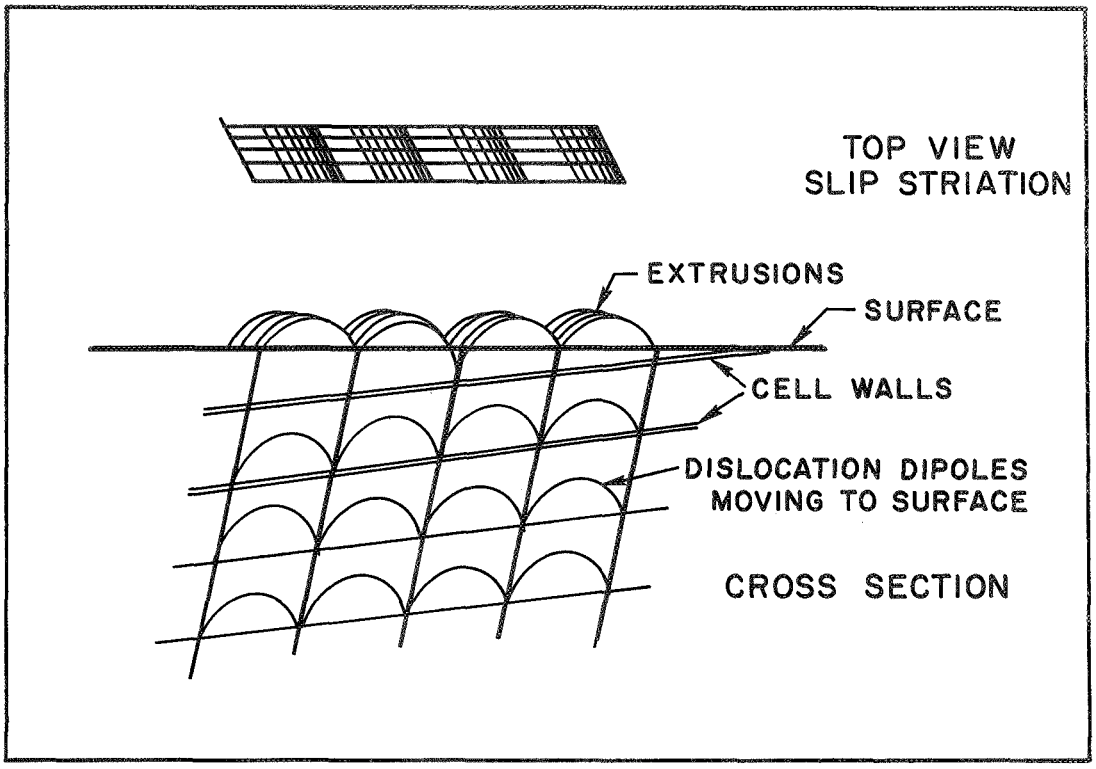

Figure 30. Geometry of cells which lead to braided extrusions.

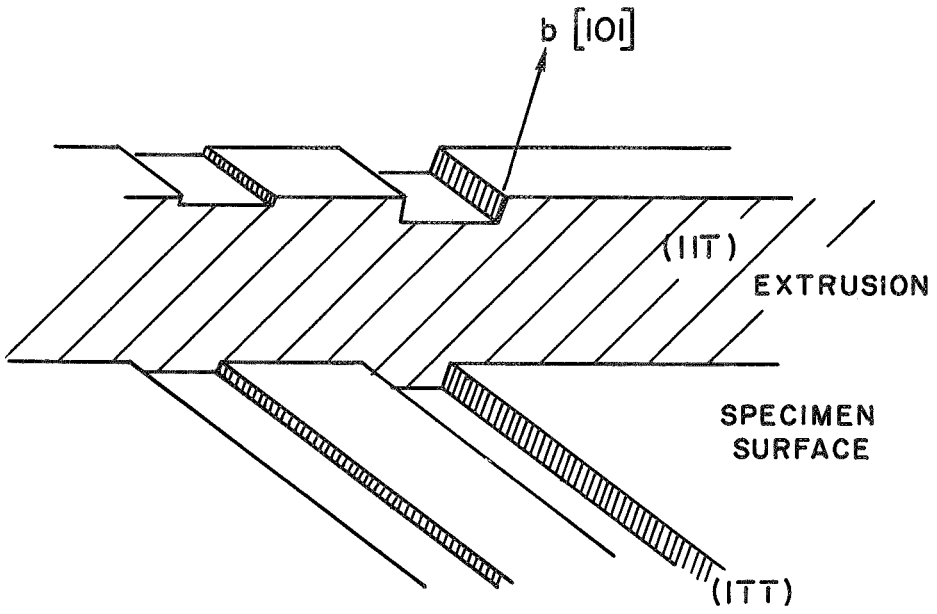

a

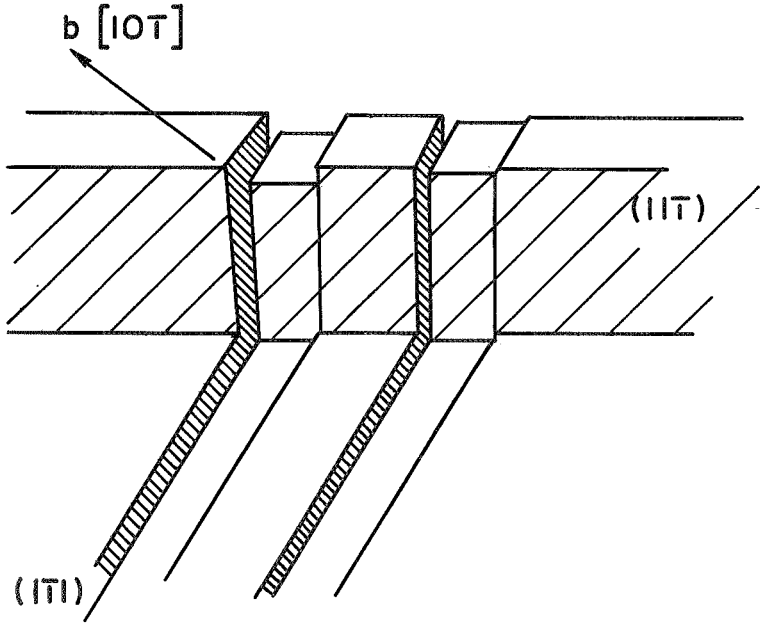

b

Figure 31. (a) Effect of dislocation with Burgers vector in plane of extrusion

(b) effect of dislocations with Burgers vector not in the plane of the extrusion.

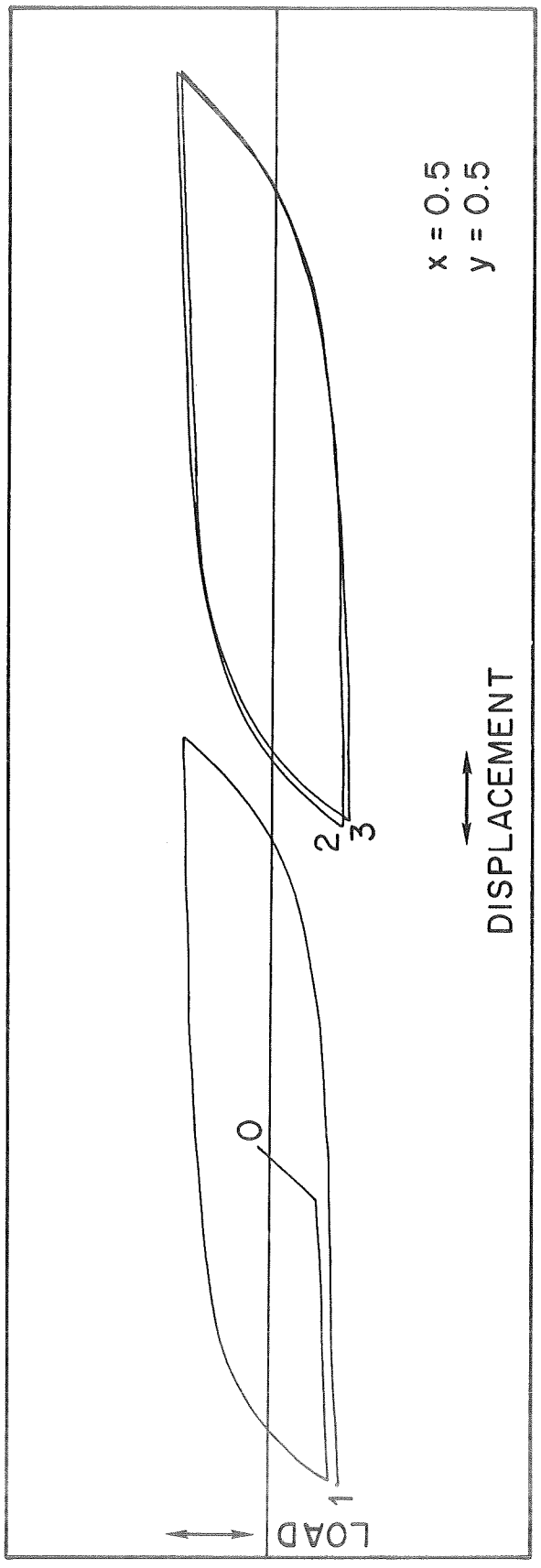

Figure 32. Hysteresis loops for specimen 18.

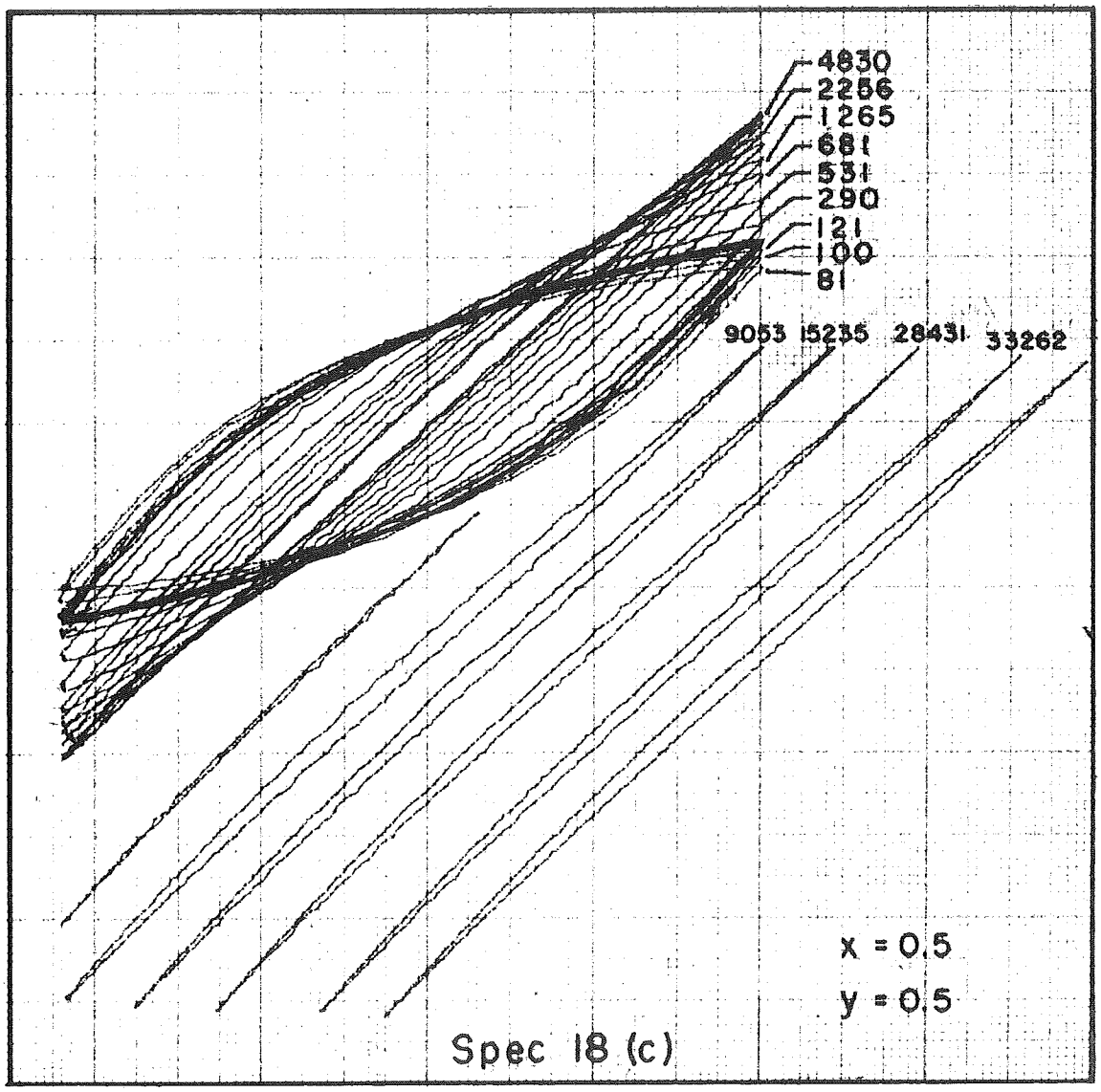
4830
2256
1265
681
531
290
121
100
81
9053
15235
28431
33262
x = 0.5
y = 0.5
Spec 18 (c)

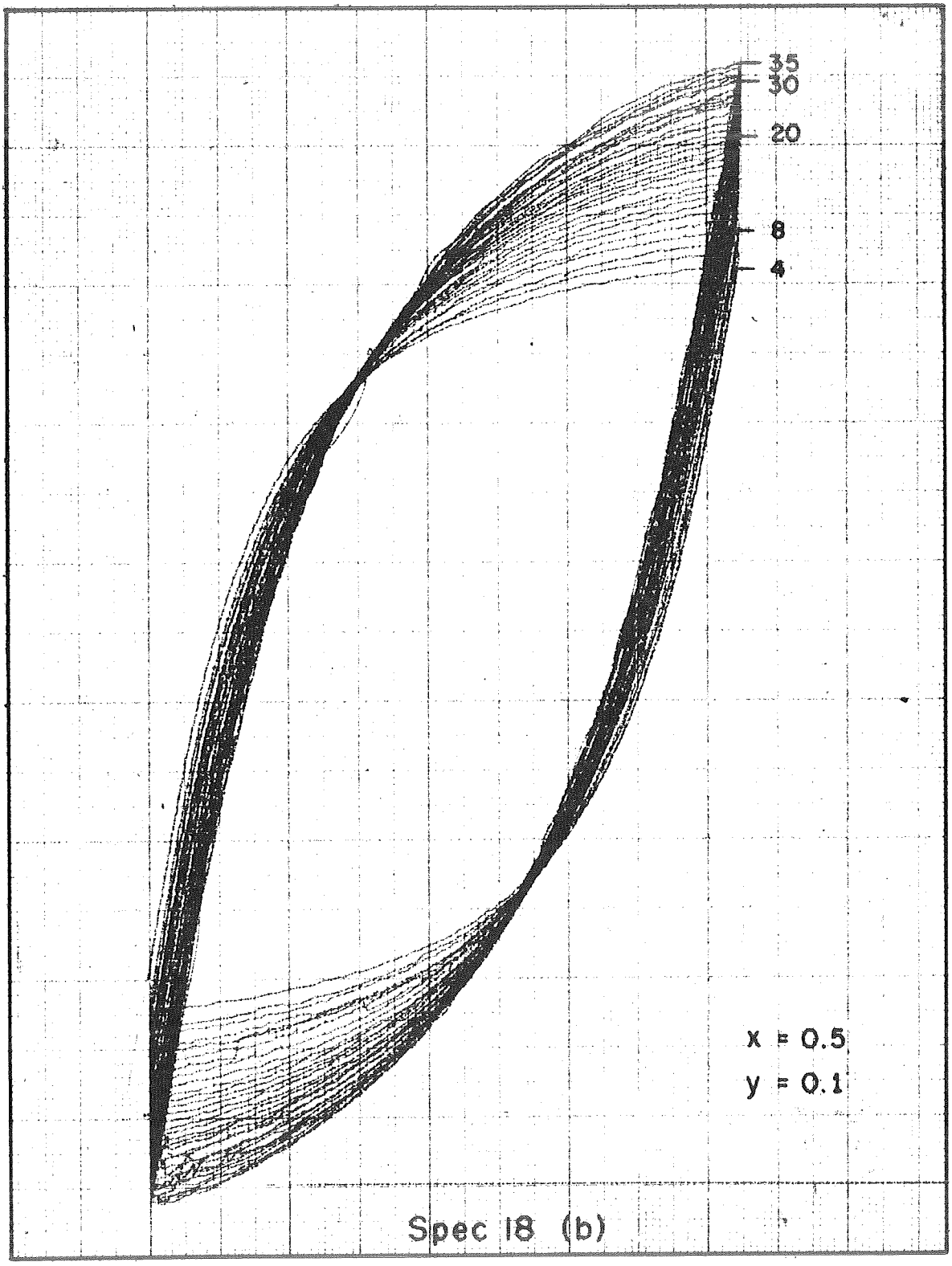
35
30
20
8
4
x = 0.5
y = 0.1
Spec 18 (b)

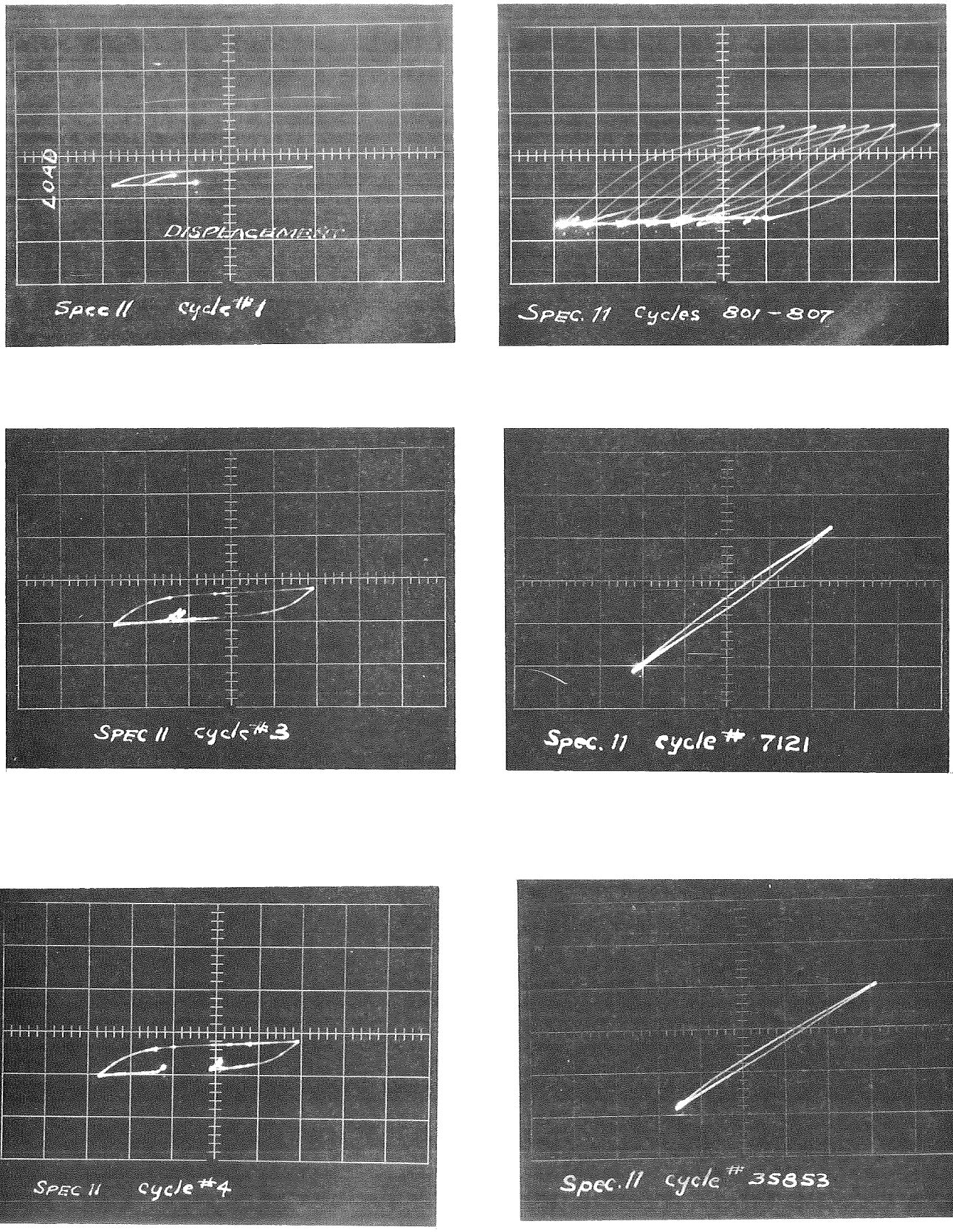

Figure 33. Oscilloscope photographs of hysteresis loops.

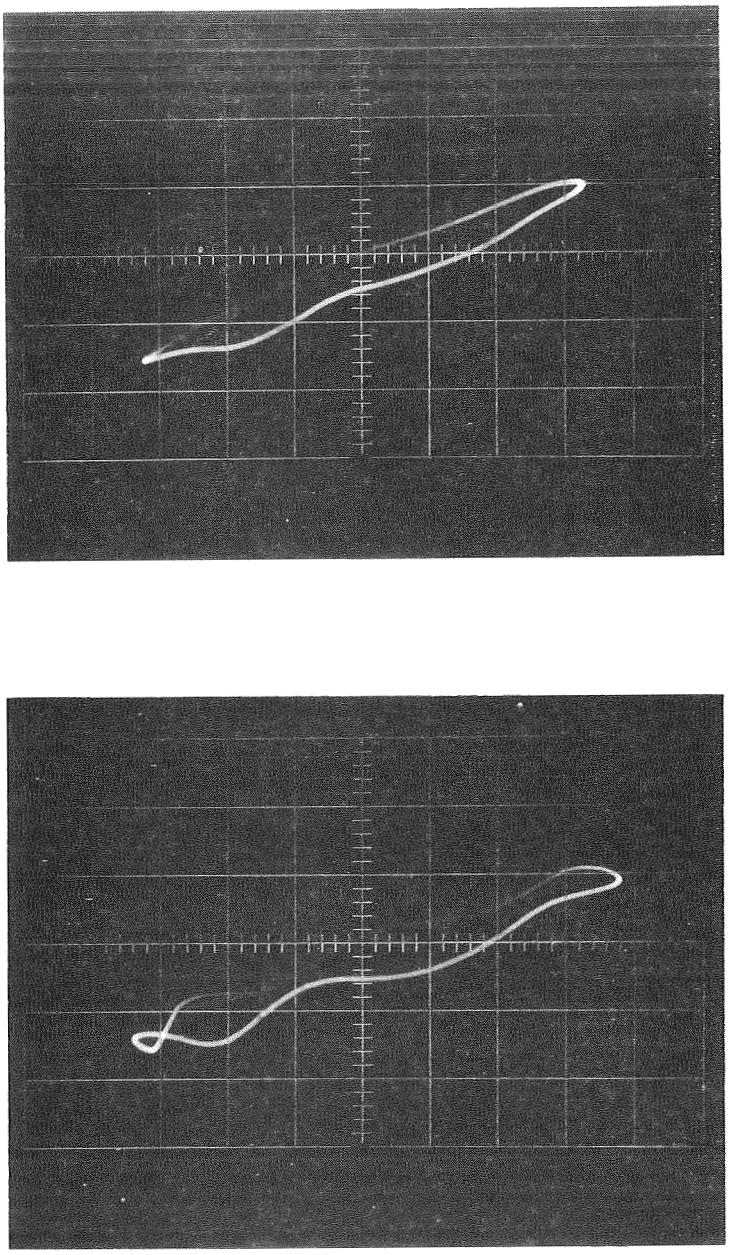

Figure 34. Dynamic hysteresis loops, frequency 50 cps.

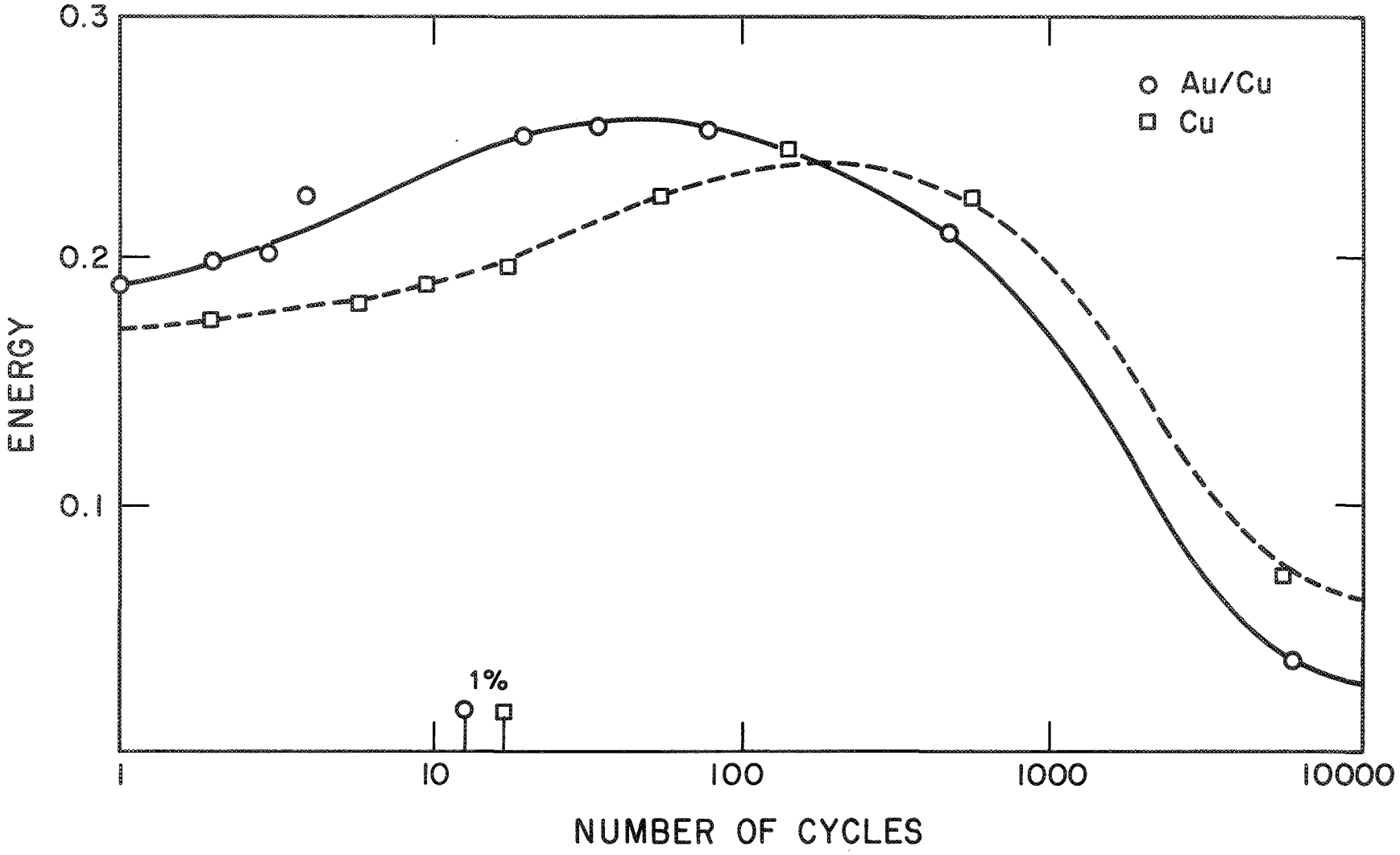

Figure 35. Load vs. number of cycles of constant strain.

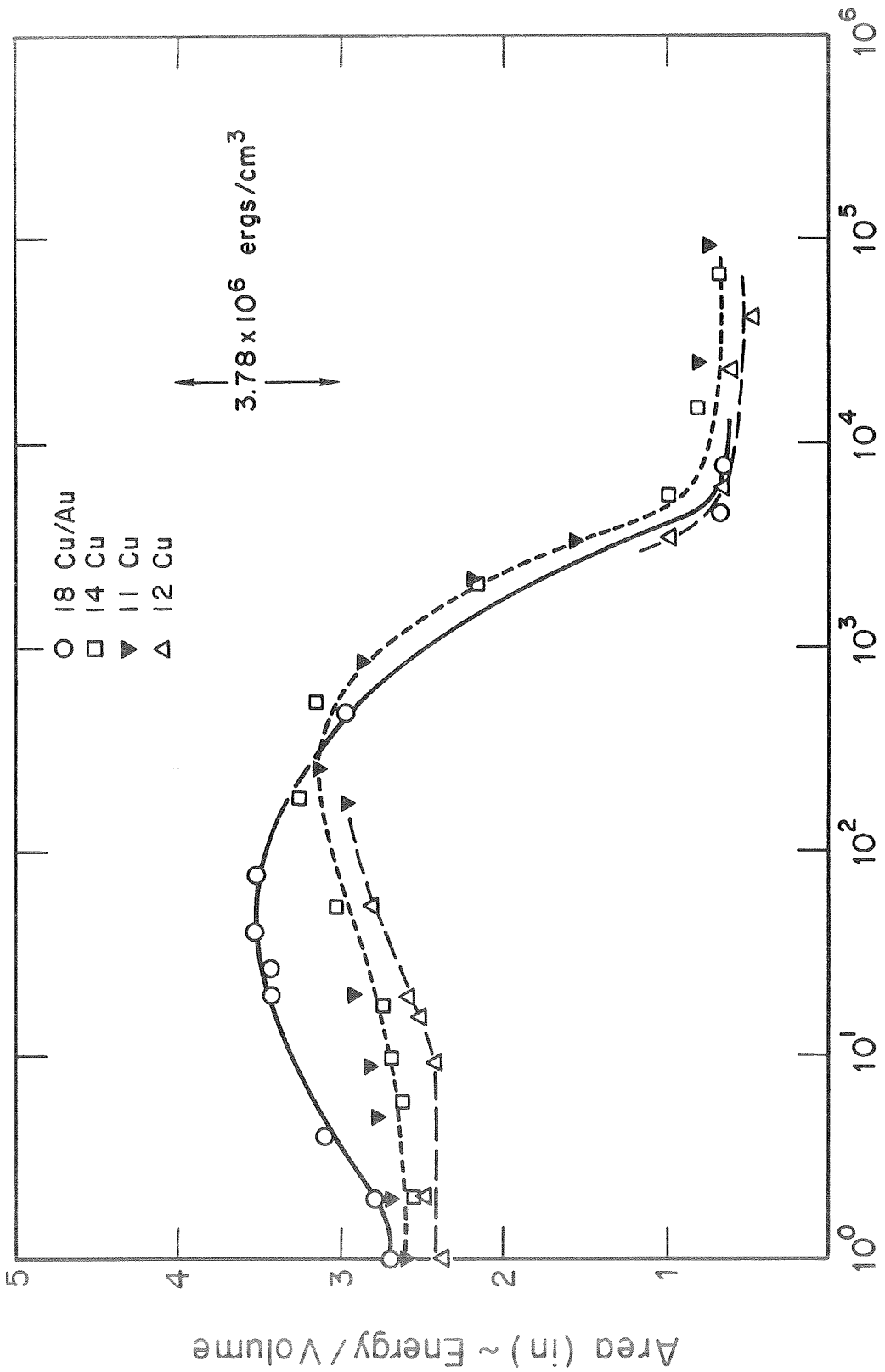

Figure 36. Change in energy loss as a function of number of cycles.